CHALMERS

Design and Evaluation of the Vienna Rectifier for a 5MW Wind Turbine System

Master of Science Thesis

MOJGAN NIKOUEI

Department of Energy and Environment

Division of Electric Power Engineering

CHALMERS UNIVERSITY OF TECHNOLOGY

Gothenburg, Sweden 2013

Design and Evaluation of the Vienna Rectifier for a 5MW Wind Turbine System

Mojgan Nikouei

Department of Energy and Environment
Division of Electric Power Engineering
CHALMERS UNIVERSITY OF TECHNOLOGY
Gothenburg, Sweden 2013

Design and Evaluation of the Vienna Rectifier for a 5MW Wind Turbine System

Mojgan Nikouei

Design and Evaluation of the Vienna Rectifier for a 5MW Wind Turbine System

Mojgan Nikouei

Department of Energy and Environment

Division of Electric Power Engineering

Chalmers University of Technology

Abstract

This thesis is a part of a larger project that deals with the design of an offshore DC wind turbine system. The aim of this thesis is to design and evaluate the Vienna rectifier for a 5 MW wind turbine system (WTS) with a permanent magnet synchronous generator (PMSG). In order to estimate the efficiency and the maximum power of the rectifier's generator that can be extracted, the power losses have to be calculated and suitable power electronic switches should be chosen. Finally, the results are to be compared with the performance of the diode rectifier and the conventional IGBT converter.

Generally, the Vienna rectifier is applied to many applications with high switching frequency such as a power supply for an electronic system, especially for telecommunication devices. However, in this project, an effort is made to use it in a wind turbine system application, which has a low switching frequency. The idea behind is to enhance the pure diode rectifier and in this way extract more output power. Therefore, to investigate the performance of the Vienna rectifier and design it according to the project's requirements, several steps have been done.

In the first part, the rectifier operation is studied. The Vienna rectifier is a three phase, three levels and three-switch rectifier; it is a kind of PWM (Pulse Width Modulation) with a partly controlled output voltage.

There is a midpoint N, between two equal dc voltages at the output DC bus voltage, which is considered as a reference point with zero voltages. Therefore, three different voltages, $+\frac{V_0}{2}$, 0, $-\frac{V_0}{2}$ are available as output. Based on the phase current direction and the state of the switches, the phase potentials voltages could be determined. An important point in controlling of the Vienna rectifier is the phase displacement angle φ_s. According to available literature, it has the limitation between $(-\frac{\pi}{6}, +\frac{\pi}{6})$. However, it is shown here that this is not completely true in this application.

In the next part, the designs of the converter and the power as well as the loss calculation have been done. The circuit of the Vienna rectifier is simulated in the Simplorer software and all of the waveforms are exported to Matlab in order to do the calculations. The simulation results show that the Vienna rectifier has low losses partly due to a very low switching frequency. The IGBTs are turned on only twice during one line period. When the IGBT is in the ON state position during a half period, the output power that can be extracted is 5 MW with a 43° phase shift angle. This power is extracted when the output dc-link voltage has the value, 9100 V. As the Vienna rectifier can work in a wide voltage range, other dc voltages are examined. Simulations are performed for, 4300 V, 8400 V, 9100 V and as expected, the Vienna rectifier has the similar operation with diode rectifier at 4300 V. The pure diode rectifier that works with the same generator can only provides 2.5 MW if no extra capacitors are used.

Due to usage of only three IGBTs in designing the Vienna rectifier, the voltage stress during blocking of power electronic switches would be reduced, as well as manufacturing cost, in comparison with the conventional IGBT converter.

Acknowledgments

Contents

Table of contents

List of Nomenclatures

The following list presents nomenclatures that are used throughout this thesis

P_{mec}	Mechanical power extracted from the wind
ρ_{air}	Air density
A_r	Area swept by the rotor
C_p	Power coefficient
ω_{wind}	Wind speed
λ	The tip speed ratio
ω_r	Rotor blade speed.
i_d	Stator current in d axis
i_q	Stator current in q axis
u_{sd}	Stator voltage in d axis
u_{sq}	Stator voltage in q axis
p	Pole pairs
ψ_m	Amplitude of the flux induced by permanent magnets of the rotor in the stator
R_s	Resistance of the stator windings
L_d	Stator inductance in d axis
L_q	Stator inductance in q axis
$\angle \vec{u_s}$	Angle of machine voltage relative to machine position
$\angle \vec{i_s}$	Angle of machine current relative to machine position
φ	Phase difference of inverter output voltage and current
L_N	Input inductors
i_k	Phase current
E_N	Input voltage
V_{KN}	Phase potential
V_0	DC-link voltage
P_{loss}	Total power loss
P_{sw}	Switching loss
P_{cond}	Conduction loss
V_{on}	Forward voltage drop
r_{on}	On state resistor
E_{on}	Energy during the turn-on,
E_{off}	Energy during the turn-off
i_C	IGBT collector current
v_{CE}	IGBT collector Emitter voltage
I_{ref}	IGBT reference current
V_{ref}	IGBT reference voltage
v_R	Diode reverse recovery voltage
i_R	Diode reverse recovery current
I_F	Forward current before the turn-off
I_{rr}	Reverse recovery current,
Q_{rr}	Reverse recovery charge
t_{rr}	Reverse recovery time
E_{rev}	Reverse recovery energy
E	Back EMF
V	Phase voltage
X	Reactance

Chapter 1

1. Introduction

1.1 Problem Background

Today, producing electrical energy by renewable sources such as wind, solar and wave are becoming very important since the demand of electrical energy is increasing rapidly and the fossil fuel sources are limited. Among these renewable sources, wind is highly popular and wind conversion systems technology already plays an important role in power production. Since power is proportional to the cube of wind speed [6], the location of wind turbine becomes important. Therefore, building offshore wind farm is a good alternative to extract maximum power due to high average wind speed. Other advantages that make offshore wind farm attractive are mitigation of noise and visual impact problems, since the park is located far away from where people continuously are. On the other hand, high construction cost and maintenance are disadvantages of offshore wind farms.

Due to the above given motivations, the numbers of offshore wind farms that include several wind turbines is increasing. The transmission of electrical power for such a long distance from offshore to the consumer becomes a problem due to the reactive power generation in the AC cable technology. HVDC systems cannot only solve this transmission problem, but can also make a reduction in loss during power transmission. In case of using HVDC, traditional 50 Hz transformers could be replaced with converters.

By careful design of the power electronics, the power production cost can be reduced. Basically, the main ability of the power electronics is improving the control of the wind turbine system and also to improve the connection to the grid system.

Low weight of the components in converters as well as newer power electrical semiconductors with lower losses are the other reasons that make them attractive in wind turbine systems.

In the classical system with a two level six-pulse converter the six switches operate with high frequency. It would be a great advantage if we could have a few IGBTs and less switching of IGBTs. Therefore, this thesis will investigate a "Vienna rectifier for a 5 MW wind turbine application".

1.2 Previous Work

This thesis is a part of a project that is to design an offshore DC wind park system. The project is divided into three main parts,

- Investigating different generating systems with low, medium or high speed generators for offshore wind turbines with HVDC transmission lines. Further, estimating energy efficiency and determining weight and cost for the different generators with different AC\DC rectifier. Moreover calculating life cycle cost for various systems.
- Designing a DC\DC converter including "High Frequency High power Transformer"
- Designing a meshed dc network, with wind farms connected to it.

In a previous Master Thesis [2], a diode rectifier for a 5 MW wind turbine with a PMSG (Permanent Magnet Synchronous Generator) was designed. The efficiency of the rectifier as well as the power extraction of that system was determined. Loss calculation results were compared with an active rectifier.

1.3 Purpose

The purpose of this thesis is to design and evaluate a Vienna rectifier for a 5 MW wind turbine with a PMSG, to estimate the efficiency and the maximum power extraction using this rectifier. Moreover, an objective is to choose the suitable power electronic switches for the rectifier. Further, a target is to calculate the rectifier losses. Finally, an aim is to compare the results with the diode rectifier and the conventional IGBT converter.

However, some topics such as: control topology for rectifier with PMSG, design of output filter, reactive power compensation and thermal calculation are not covered in this thesis and they are left for future work.

Chapter 2

2. Theory

2.1. Wind Turbine System

Wind turbine system operates with fixed and variable speed and the aerodynamic forces are controlled in three ways, such as stall, pitch and active stall. Based on their ability to control speed and the type of the power control; they are classified according to Table 2.1.

Table 2.1 Wind turbine system

Speed control		Power control		
		Stall	Pitch	Active stall
Fixed speed	Type A	Type A_0	Type A_1	Type A_2
Variable speed	Type B	Type B_0	Type B_1	Type B_2
	Type C	Type C_0	Type C_1	Type C_2
	Type D	Type D_0	Type D_1	Type D_2

Colored cells show the combination that is used as typical wind turbine systems while others are not used in the wind turbine industry. Among them, variable speed wind energy conversion are most commonly used due to that they allow maximum power extraction from the wind [4] as well as reduce mechanical stress and have less noise emission [2].

The mechanical power extracted from the wind can be calculated as

$$P_{mec} = \frac{1}{2}\, \rho_{air}\, A_r\, C_p \omega_{wind}^3 \tag{2.1}$$

where P_{mec} is mechanical power on the shaft of the turbine, ρ_{air} is air density, C_p is power coefficient, A_r is area swept by the rotor, ω_{wind} is wind speed[5].

The power coefficient (C_p) is a function of the pitch angle in degrees (γ) and the tip speed ratio (λ). The tip speed ratio is defined as

$$\lambda = \frac{\omega_r}{\omega_{wind}} \tag{2.2}$$

where ω_r is the rotor blade speed.

In variable speed wind turbines, ω_r is changed proportionally to the wind speed for the lower wind speed, in order to extract maximum power from the wind; λ is kept constant therefore, C_p has the value between 0.4 to 0.5 [6].

Fig. 2.1 shows all highlighted types of wind turbines in the Table 2.1.

Chapter 2. Theory
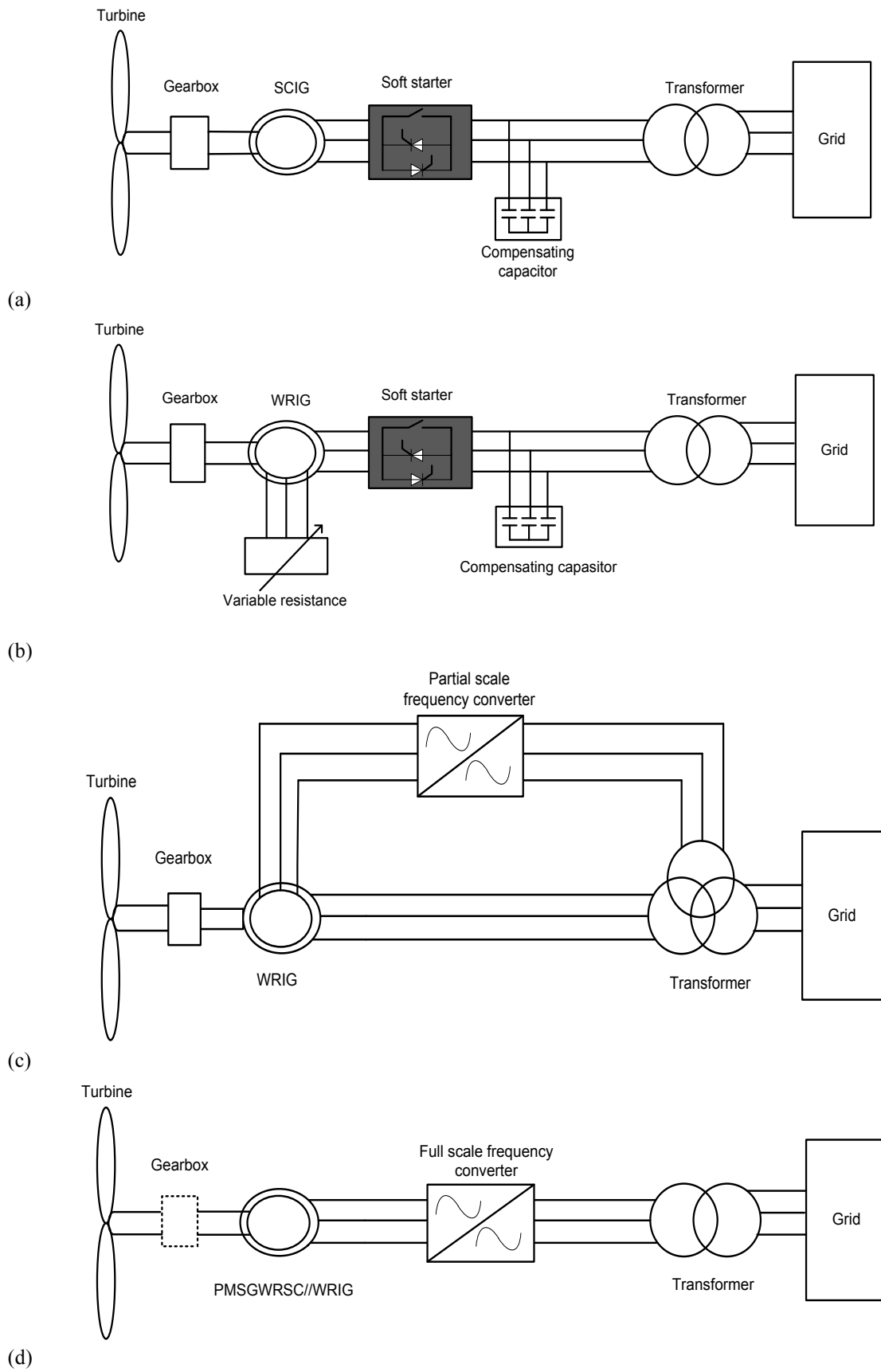

(a)

(b)

(c)

(d)

Fig. 2.1 Wind Turbine
(a) Type A (fixed speed); (b) Type B (limited variable speed); (c) Type C (variable speed with partial scale
frequency converter); (d) Type D (variable speed with full scale frequency converter)

According to Fig. 2.1, wind turbine systems consists of three main different parts; generators, converters and transformers. As is displayed, different types of generators such as the squirrel cage induction generator (SCIG), wound rotor induction generator (WRIG) and permanent magnet synchronous generator (PMSG) are used in various configurations. These days, using a PMSG is more common due to its high efficiency and reliability. Low weight and volume are the other reasons that make it popular in wind turbine systems [7]. As mentioned earlier, another important part in a wind turbine is the converter. Different common types of converters such as back to back six switch two level PWM converter or multi level converter such as back to back three level neutral point clamped are used [5] .The Vienna rectifier is such an AC\DC converter that could also be used in wind turbine system. Due to the feature of fewer switches it could decrease the cost and control complexity.

Here, an effort is made to investigate the using of a Vienna rectifier as AC\DC converter in a wind turbine configuration combined with a PMSG.

2.2. Permanent Magnet Synchronous Generator (PMSG)

As mentioned earlier, The PMSGs are becoming an attractive generator in a wind turbine system due to several advantages. The dq-model using amplitude invariant transformation of the PMSG is represented by the following expressions,

$$\frac{di_d}{dt} = \frac{1}{L_d}\ (u_{sd}\ + p\omega_r L_q i_q - R_s i_{sd}) \tag{2.3}$$

$$\frac{di_q}{dt} = \frac{1}{L_q}\ (u_{sq}\ - p\omega_r(L_d i_d + \psi_m) - R_s i_{sq}) \tag{2.4}$$

where L_d, L_q are stator inductances, u_{sd}, u_{sq} are stator voltages, i_{sd}, i_{sq} are stator currents in d and q axis, ω_r is the rotor speed, p is the pole pairs, ψ_m is amplitude of the flux induced in the stator by the permanent magnets in the rotor, R_s is the resistance of the stator windings[9].

2.3. Vienna Rectifier Principal

The Vienna rectifier was introduced in 1993 by Prof. Johann W. Kolar [10]. It is a three phase, three levels and three switch rectifier; it is kind of PWM (Pulse Width Modulation) rectifier with controlled output voltage. The topology of the Vienna Rectifier is a combination of a boost DC\DC converter with a three-phase diode bridge rectifier. Fig. 2.2 illustrates this rectifier circuit.
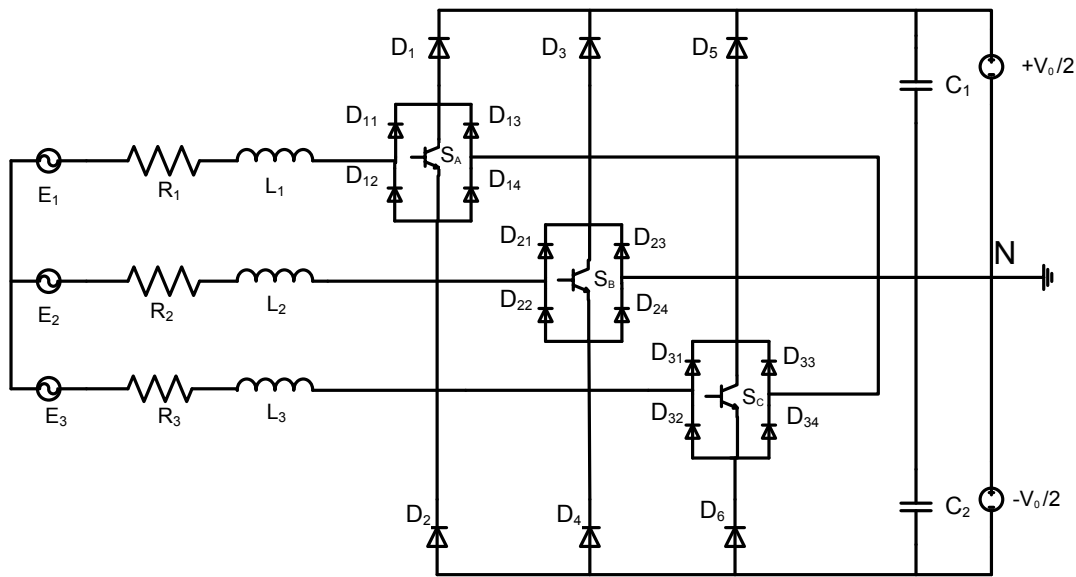
Fig. 2.2 Vienna rectifier

As Fig. 2.2 shows, the output capacitor is split in two parts with two equal values (C_1 and C_2). Across each capacitor, two voltage sources $+V_0/2$ and $-V_0/2$ exist which detect the output voltage of the circuit. Therefore three different voltages ($+V_0/2$, 0, $-V_0/2$) are available. The DC bus voltage is assumed to be a constant dc voltage [11] and can be connected to a conventional six switch or other type of inverter [12].

The input current for each phase is defined by the voltage applied across the corresponding inductor L_N; the input voltage of the rectifier is determined by the switching state and the input current direction. The input inductors (L_N) charge when the switch is on and the current increase in the inductor, and when the switch is off the inductors discharge through the positive or negative diode depending on the current flow direction. The existence of an input inductor creates a current source at the input while the capacitors create output voltages. In other words, the Vienna rectifier may be considered as a diode–transistor matrix connecting the input current sources with output voltages [13]. Fig. 2.3 shows an equivalent schematic diagram for the Vienna rectifier.
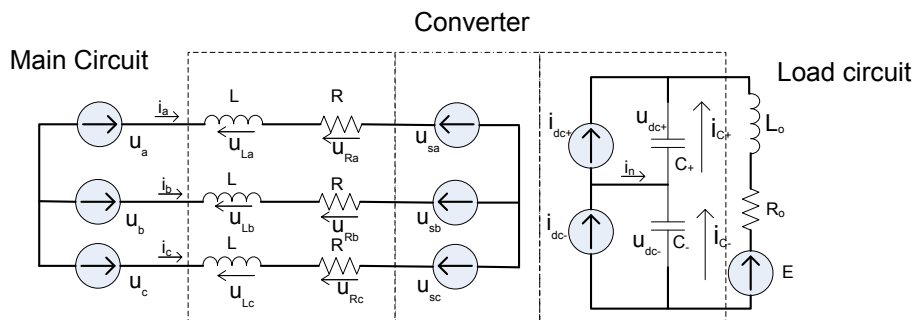

Fig. 2.3 Vienna rectifier equivalent schematic diagram

The Vienna rectifier like all the other converters in power electronics has advantages and disadvantages. The pros of this converter are given below,

- Has continuous sinusoidal input current
- No need for a neutral wire
- Low number of IGBTs used
- Low manufacturing cost
- Reduce blocking voltage stress on power semiconductor (in comparison with two level converters it becomes half because there is only one switch existing on one phase leg of the rectifier. This result would be true if the neutral point is completely balanced; however the neutral operating point operating imbalance, the capacitor voltage will exceed half of dc-link voltage and in this case, the voltage stress on the switches will increase, therefore the neutral point is an important topic in three system level converter [14]).
- Reduction in switching loss of the power semiconductors by almost 40% [15].
- Wide voltage range [15].
- Higher efficiency.
- Boosting ability.
- Production of three levels of voltage with two equal DC voltages.

On the other hand, acting as a unidirectional active AC\DC converter and lack of regeneration can be considered as cons. In unidirectional converters power flows in one direction from AC side to DC side and it cannot act as an inverter.

2.4. Operation of the Vienna Rectifier

The Vienna rectifier has three switches, and by choosing their (ON\OFF) state considering the polarity of the phase current in each phase, the voltage for each phase will be determined. So, the phase voltage is depending on the direction of phase current and switch position. In this topology, the midpoint N is considered as reference point with zero voltage. Therefore, the phase voltage is described as,

$$L_N \frac{di_k}{dt} = E_N - V_{KN} \tag{2.5}$$
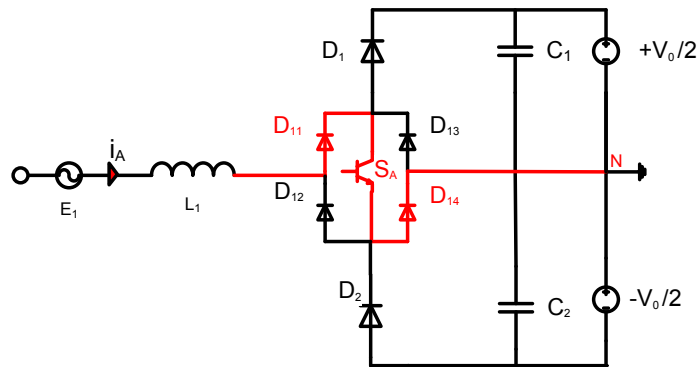
when the phase current is positive,

$$V_{KN} = \begin{cases} \dfrac{+V_0}{2} & S_k = 0 \\ 0 & S_k = 1 \end{cases} \tag{2.6}$$
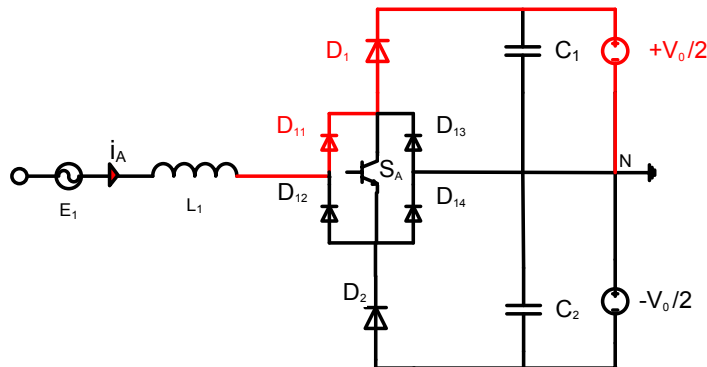
and when the phase current is negative,

$$V_{KN} = \begin{cases} \dfrac{-V_0}{2} & S_k = 0 \\ 0 & S_k = 1 \end{cases} \tag{2.7}$$

where L_N are the input inductors (N=1,2,3), i_k is the input phase current, V_{KN} is the phase voltage (K =A,B,C), S_k is a controlled switch ($S_k = 0$ correspond to off state and $S_k = 1$ to the on state).
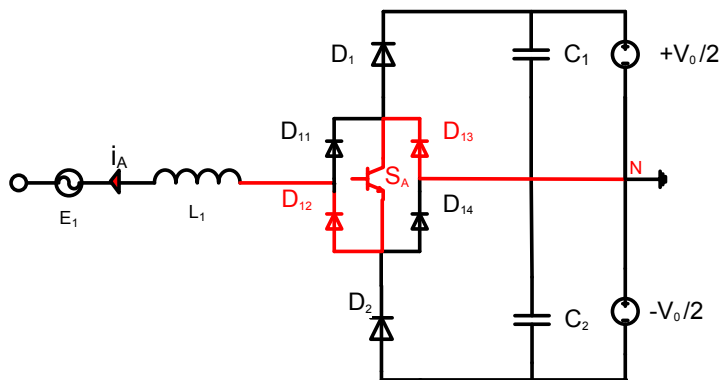
Fig. 2.4 shows the behavior of phase A. Phases B and C behave the same pattern.
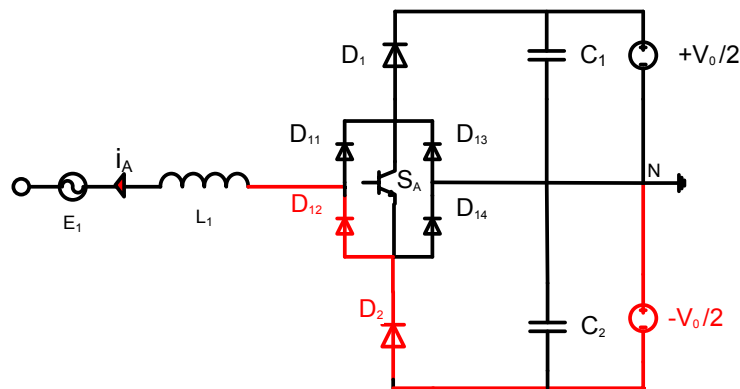

(a) line current is positive and S_A is ON

(b) line current is positive and S_A is OFF

(c) line current is negative and S_A is ON

(d) line current is negative and S_A is OFF

Fig. 2.4 Conduction path for phase A

If the line current is positive and switch S_A is ON (Fig. 2.4(a)); the current pass through the switch and the phase voltage (V_{AN}) become zero. If the polarity of the current remains as before but the control switch S_A is off, the current flows through diode D_{11}, the voltage V_{AN} is $+V_0/2$, Fig. 2.4(b) illustrates this case. Similarly, the voltage V_{AN} can determined if the line current is negative and switch S_A is ON or OFF, the current path for these two cases is illustrated in Fig. 2.4 (c), (d) [7].

The current path for two example switching position, 110 and 001, are shown in Fig. 2.5.
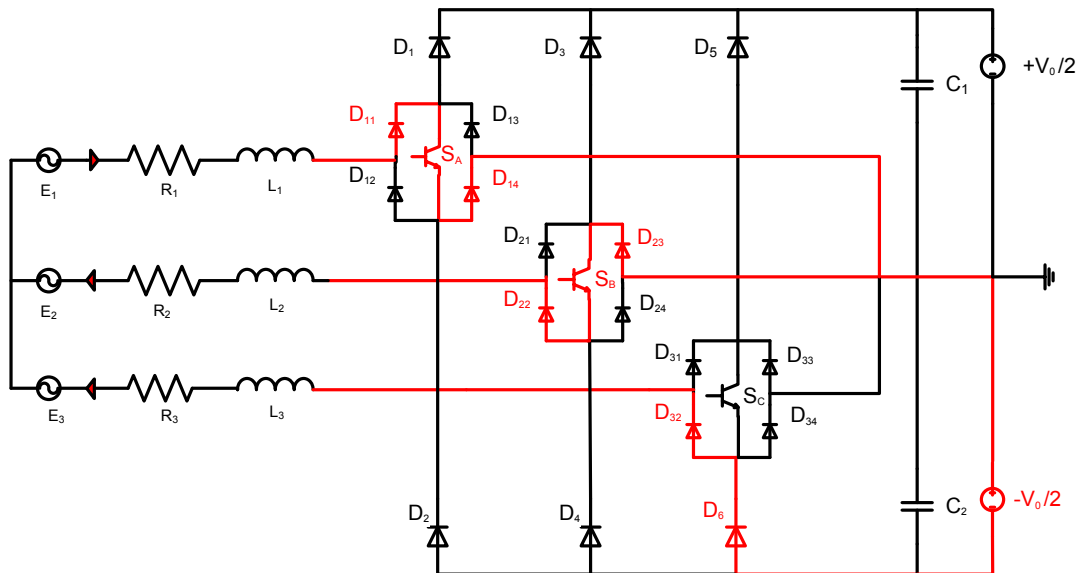
(a) 110
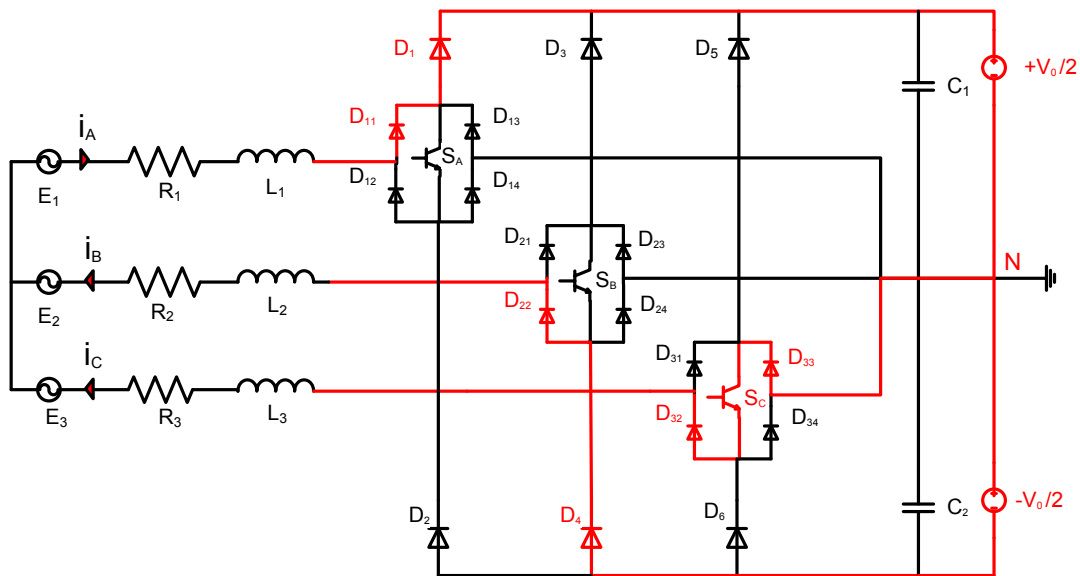
(b) 001

Fig. 2.5 The current path for two switching position

If it assumed that the current for phase A is positive and it is negative for both phase B and C. Then eight different switching positions can be considered, given the results shown in Table 2.2.

Table 2.2 Eight different switching combination

S_A	S_B	S_C	V_{AN}	V_{BN}	V_{CN}
0	0	0	$+V_0/2$	$-V_0/2$	$-V_0/2$
0	0	1	$+V_0/2$	$-V_0/2$	0
0	1	0	$+V_0/2$	0	$-V_0/2$
0	1	1	$+V_0/2$	0	0
1	0	0	0	$-V_0/2$	$-V_0/2$
1	0	1	0	$-V_0/2$	0
1	1	0	0	0	$-V_0/2$
1	1	1	0	0	0

2.5. Voltage Space Vector

As mentioned before, the voltage space vector is one way to visualize the Vienna rectifier's output voltage for different switching patterns. The basic voltage space vector is consisting of six zones where the current signs can have different values.

$$Zone = \begin{cases} 0 & if \; i_A = positive \; ; i_B = negative; i_C = negative; \\ 1 & if \; i_A = positive \; ; i_B = positive; i_C = negative; \\ 2 & if \; i_A = negative \; ; i_B = positive; i_C = negative; \\ 3 & if \; i_A = negative \; ; i_B = positive; i_C = positive; \\ 4 & if \; i_A = negative \; ; i_B = negative; i_C = positive; \\ 5 & if \; i_A = positive \; ; i_B = negative; i_C = positive; \end{cases} \tag{2.8}$$

Each of these zones describes one hexagon in the $\alpha\beta$ refrence frame and is settled with a $\frac{\pi}{3}$ difference angle with respect to each other. Each hexagon consists of eight different switching combinations; e.g. Table 2.2 refers to zone 0. Fig. 2.6 describes these zones.
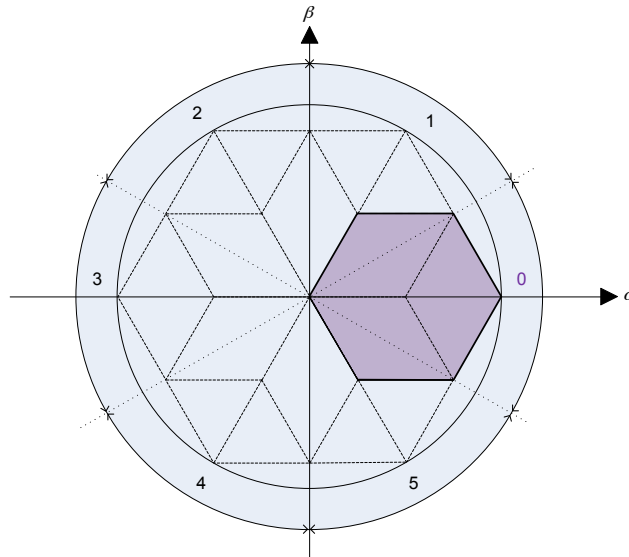

Fig. 2.6 Voltage base space vectors of the Vienna rectifier

An important point in the controlling of the Vienna rectifier is the phase displacement angle (φ_s). This angle is defined between the fundamental current and the fundamental voltage at the AC side of the converter. φ_s's limit is described as follows [16]

$$-\left(\frac{\pi}{6}\right) \leq \varphi_s \leq +\left(\frac{\pi}{6}\right) \tag{2.9}$$

2.6. Semiconductor Components in the Vienna Rectifier

2.6.1 Diode

Diodes are the simplest devices among the entire power semiconductors. The pn-junction as shown in Fig. 2.7 is the basic building block for all the other power semiconductors. Generally, it consists of the three layers with different doping and thickness. The first layer is a heavily doped n-type, n^+ that formed the cathode. On the top of that, is a layer of lightly doped n-type, n^- that is called drift region and finally a heavily doped p-type, p^+ layer on top, is forming the anode.
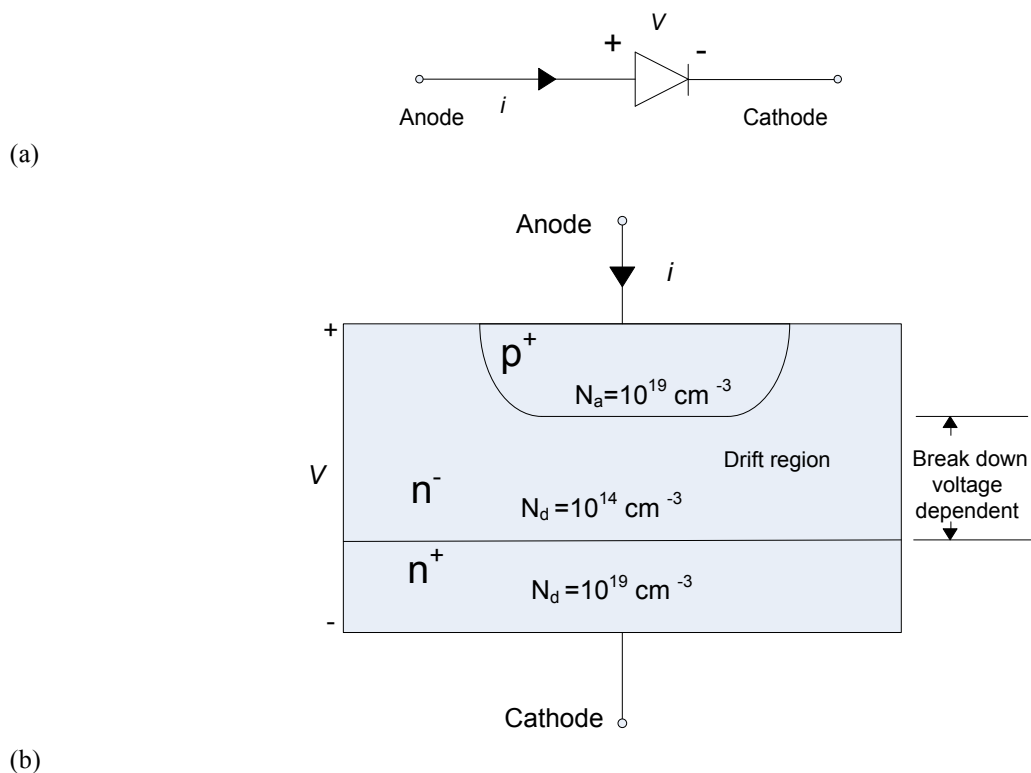

(a)

(b)

Fig. 2.7 (a) diode circuit symbol.(b) Cross-sectional view of a pn-junction diode

The diode's cross sectional area depends on the amount of current that the device is designed to carry. Diodes always conduct the current in one direction, from the anode to the cathode. As the i-v characteristic (Fig. 2.8) shows, when the applied voltage over the diode is greater than a definite forward threshold voltage (about 1 V), the diode starts to conduct and the current grows linearly. When the diode is reversed biased or the voltage across the diode is less than the forward threshold voltage, then the diode blocks the current. In the ideal case, the forward voltage drop can be considered zero and the ideal characteristic curve is obtained.

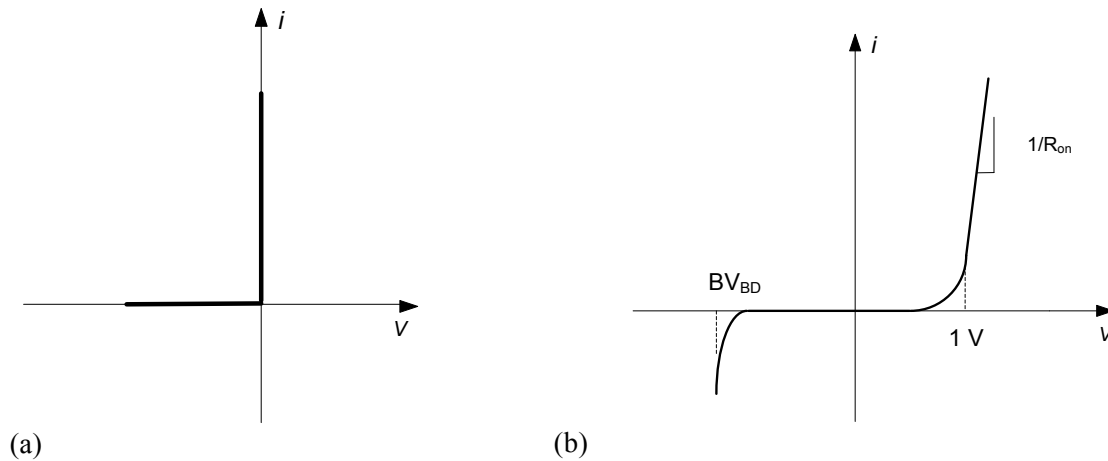(a)   (b)

Fig. 2.8 The i-v characteristic of a pn-junction diode (a) the idealized (b) the actual

In normal operation, the diode works in the both forward biased region which is called conduction region and the reverse blocking region. In the later region, a small leakage current flows as the voltage becomes more negative until the reverse voltage reaches the breakdown voltage of the diode.

When the diode is switched off, a negative current occurs as shown in Fig. 2.9. This negative current sweeps out excess carriers in the diode and allows it to block a negative polarity voltage. This process takes a short time which is called reverse recovery time. The reverse recovery current I_{rr} and reverse recovery time t_{rr} of the diode increases with increasing carrier lifetime [23].
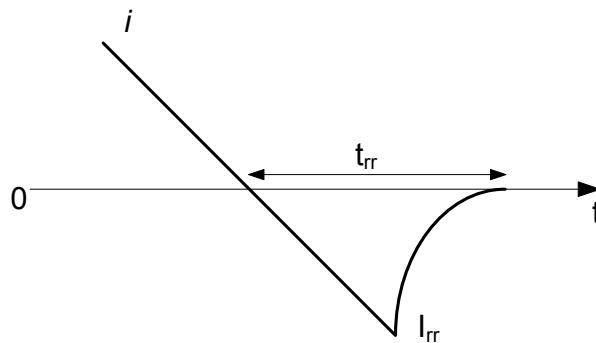

Fig. 2.9 Reveres recovery

2.6.2 IGBT

The insulating gate bipolar transistor IGBT is one of the power semiconductor devices, which are created by the combination of the bipolar junction transistor BJT and the MOSFET. Each of these power semiconductors has particular characteristics; the combination of them can make a good trade off of both. For example, BJTs have low voltage drop in the on state but have longer switching times, especially at turn-off. The MOSFETs can be turned on and off fast due to small gate capacitance, but their on-state conduction losses are higher in comparison with BJTs at the same rating [23]. Therefore, the combination gives low conduction loss and fast switching, which is the unique character of the IGBT.

Fig. 2.10 shows a vertical cross section for n-channel IGBT and its symbol. The structure is quite similar to the MOSFET. The p^+ layer forms the drain while the n^+ layer forms source.
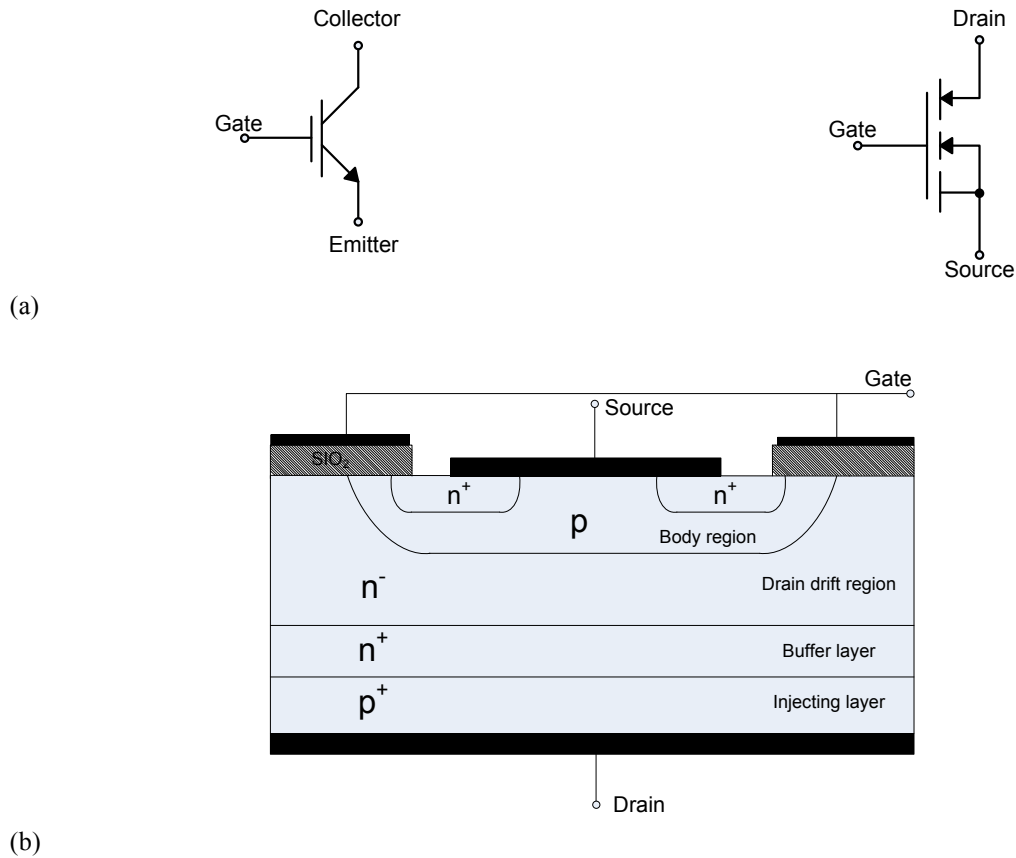
Collector

Gate

Emitter

Drain

Gate

Source

(a)

Gate

Source

SiO₂

n^+

n^+

p

Body region

n^-

Drain drift region

n^+

Buffer layer

p^+

Injecting layer

Drain

(b)

Fig. 2.10 (a) The n-channel IGBT circuit symbols. (b) Cross-sectional view of an IGBT

Fig. 2.11 shows the i-v characteristic of the n-channel IGBT. In the forward direction it looks similar to the BJTs, but with a difference being in the way it is controlled. The IGBTs are controlled with input voltages, the gate–source voltage, while the input current is the controlling parameter for the BJTs. The reverse blocking voltage can be as large as the forward blocking voltage if the structure is made without n^+ layer. However, if the n^+ layer is used in the construction, the breakdown voltage is lowered significantly.
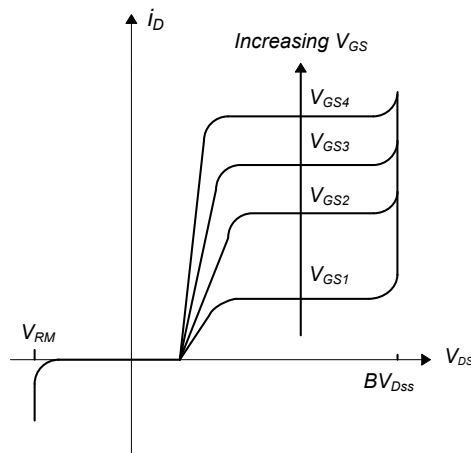
i_D

Increasing V_{GS}

V_{GS4}

V_{GS3}

V_{GS2}

V_{GS1}

V_{RM}

V_{DS}

BV_{Dss}

Fig. 2.11 The i-v characteristic of an IGBT

Fig. 2.12 shows the switching characteristic for the IGBTs, which are similar to the MOSFETs. The power dissipation appears during the turn-on switching period. The faster turn-on switching helps to reduce that power dissipation. The IGBT's turn-off switching curves are shown in Fig. 2.13 and there is a difference in the drain current waveform compares with the MOSFET. In the IGBTs, the drain current consists of two time intervals. During the first time interval, t_{fi1}, the rapid drop corresponds to the turn-off of the MOSFET section of the IGBT. The second time interval, t_{fi2}, corresponds to the BJTs and is due to the stored charges in the n⁻ drift region.
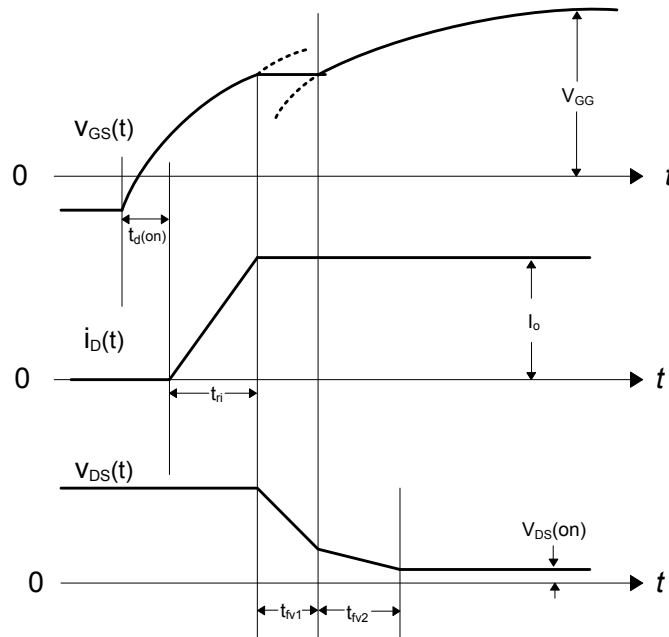

Fig. 2.12 Turn-on voltage and current waveforms of an IGBT
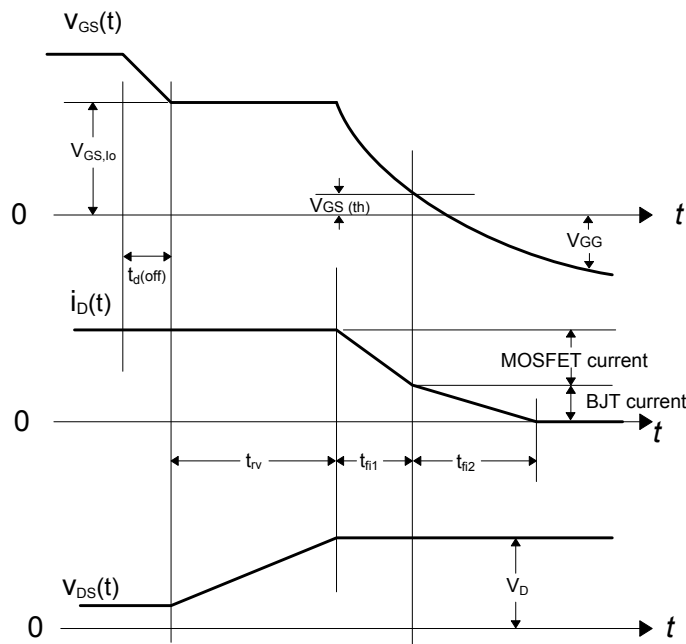

Fig. 2.13 Turn-off voltage and current waveforms of an IGBT

2.7. Power loss

Losses in power electronics are important features that determine the efficiency. Among different types of losses in the power electronic switches, only switching losses and conduction losses are considered in this project and other types of losses such as: gate driver losses, capacitor losses and snubber's losses are ignored. The losses can thus be written as

$$P_{loss} = P_{sw} + P_{cond} \tag{2.10}$$

where P_{loss} is the total power loss in the converter, P_{sw} is the switching loss in the IGBT or diode and P_{cond} is the conduction loss in the IGBT and diode.

Conduction losses can be calculated by the use of a forward voltage drop component (V_{on}) and an on-state resistor (r_{on}).

$$V_{(IGBT/diode)on} = v_{(IGBT/diode)chip} + i_{(IGBT/diode)}r_{on} \tag{2.11}$$

$$P_{cond} = \frac{1}{T}\int_0^T v_{(IGBT/diode)on}\, i_{(IGBT/diode)} \tag{2.12}$$

The IGBT/diode on-characteristics can be represented by a slope corresponding to the on-state resistor, r_{on}, and a turn-on offset [17] [18].
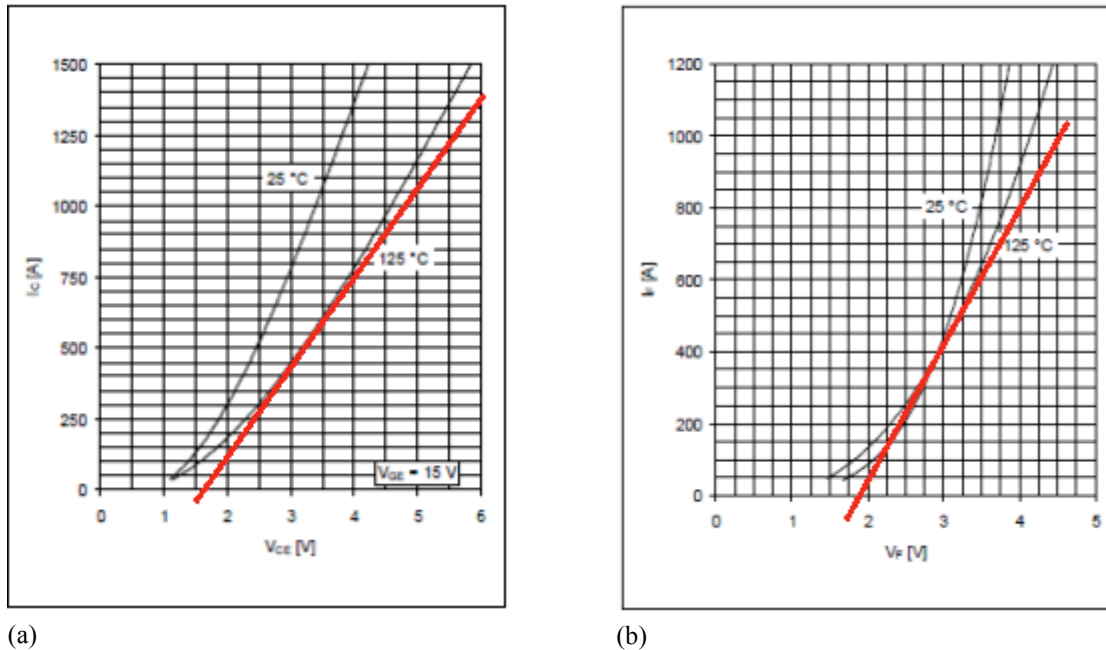

(a)   (b)

Fig. 2.14 Typical forward characteristic $(r_{on} = {\Delta V}/{\Delta I})$
(a)forward characteristic IGBT, (b)Forward characteristic diode

Switching loss is created due to the turn-on and turn-off of the IGBT or diode, and is determined as,

$$P_{sw} = (E_{on} + E_{off})/T \tag{2.13}$$

where E_{on} is the energy during the turn-on, E_{off} is the energy during the turn-off, T is the time period.

The following equation shows that in the IGBTs E_{on} and E_{off} depends on turn-on and turn-off parameters.

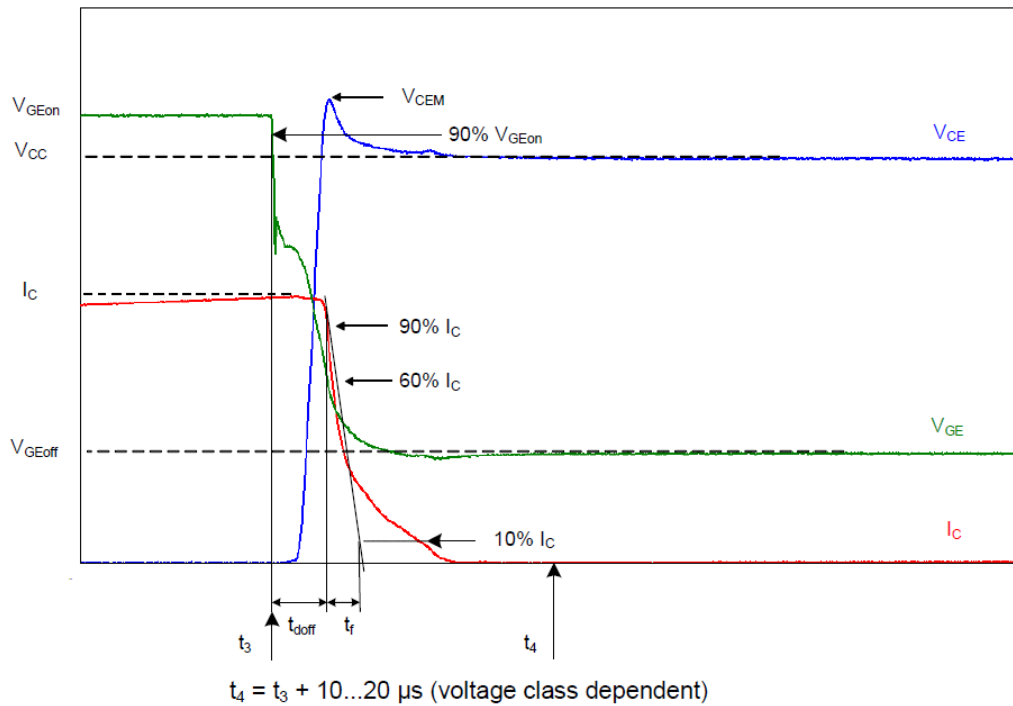$$E_{on} = \int_{t_1}^{t_2} (i_C(t)v_{CE}(t))dt \tag{2.14}$$

$$E_{off} = \int_{t_3}^{t_4} (i_C(t)v_{CE}(t))dt \tag{2.15}$$

where i_C is the collector current, v_{CE} is the collector emitter voltage, $t_1 to\ t_2$ is the turn-on time period, $t_3 to\ t_4$ is the turn-off time period.

Fig. 2.15 is a good explanation for turn-on and turn-off time periods [24].

(a)

$t_4 = t_3 + 10...20$ µs (voltage class dependent)
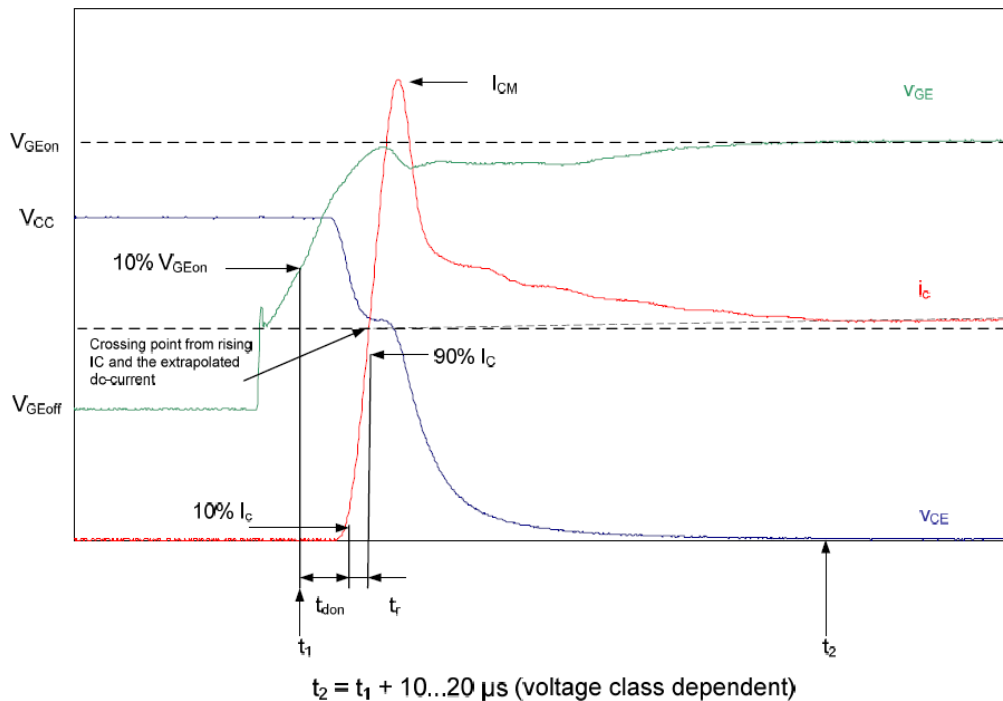
(b)

Fig. 2.15 Turn-on and turn-off parameters for an IGBT (a) Turn-on parameters (b) Turn-off parameters

Turn-on delay time, $t_{d(on)}$ is defined as time that the gate-emitter voltage rises from zero to $V_{ge(th)}$

Rise time, t_r is when the collector current has risen from 10% to 90% of its final value.

Turn-off delay time, $t_{d(off)}$ is defined as the time when the gate-emitter voltage has dropped to 90% of its initial value.

Fall time, t_f when the collector current has dropped from 90% to 10% of its initial value.

The total turn-on time is the sum of $t_{d(on)}$ and t_r , accordingly the total turn-off time is the sum of $t_{d(off)}$ and t_f .

Due to difficult calculations and inaccurate results, all information which are typically necessary to calculate switching losses such as turn-on and turn-off times and energy are typically given in the data sheet of the component [17].

Through the following relations [19], the switching losses can be recalculated from a specific current and voltage level given in the data sheet.

$$P_{sw(on)} = (E_{on}(\frac{I_{IGBT}}{\pi I_{ref}})^{K_{i_{IGBT}}}(\frac{V_{IGBT}}{V_{ref}})^{K_{v_{IGBT}}})/T \qquad (2.16)$$

$$P_{sw(off)} = (E_{off}(\frac{I_{IGBT}}{\pi I_{ref}})^{K_{i_{IGBT}}}(\frac{V_{IGBT}}{V_{ref}})^{K_{v_{IGBT}}})/T \qquad (2.17)$$

$$P_{sw} = P_{sw(on)} + P_{sw(off)} \qquad (2.18)$$

where $K_{i_{IGBT}}$ is 1, $K_{v_{IGBT}}$ is 1.35, I_{ref} is the reference current and V_{ref} is the reference voltage.

Since the diode turns on rapidly in comparison with the IGBT, the turn-on switching energy is neglected but due to reverse recovery characteristic the turn-off energy is considered as

$$E_{rev} = \int_{t_0}^{t_1} (i_R(t)v_R(t))dt \qquad (2.19)$$

Since the switching energy information in the data sheet [18] is valid, for the specific voltage and current level, the turn-off energy can be determined as [19]

$$P_{sw} = (E_{rev}(\frac{I_F}{I_{F_{ref}}})^{K_{i_{Diod}}}(\frac{V_{DIODE}}{V_{ref}})^{K_{v_{Diod}}})/T \qquad (2.20)$$

where $K_{i_{diode}}$=0.6, $K_{v_{diode}}$=0.6 and I_F is the forward current before the turn-off.

Fig. 2.16 shows the current and the voltage waveforms and corresponding switching losses for a diode during turn-off.

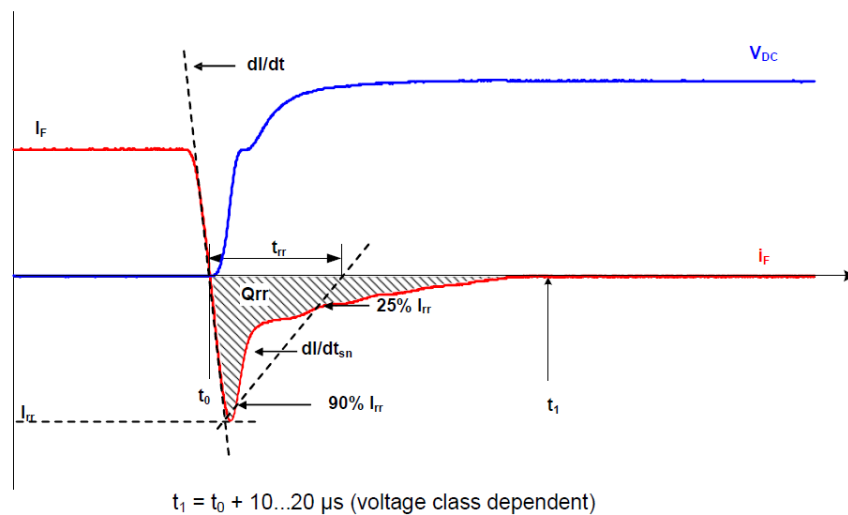$t_1 = t_0 + 10...20 \ \mu s$ (voltage class dependent)

Fig. 2.16 Turn-on and turn-off parameters for diode

where I_{rr} is the reverse recovery current, Q_{rr} is the reverse recovery charge, t_{rr} is the reverse recovery time and E_{rev} is the reverse recovery energy.

Chapter 3

3. Case Set up

In this chapter the topology of the Vienna rectifier for a 5 MW wind turbine is investigated and the component selection is described.

3.1. 5MW wind turbine with PMSG

A variable speed wind energy conversion system (WECS), consisting of a permanent magnet synchronous generator (PMSG) and a Vienna rectifier to convert mechanical power from the rotor blades to electrical energy, is used in this work. Fig. 3.1 illustrates the system topology.
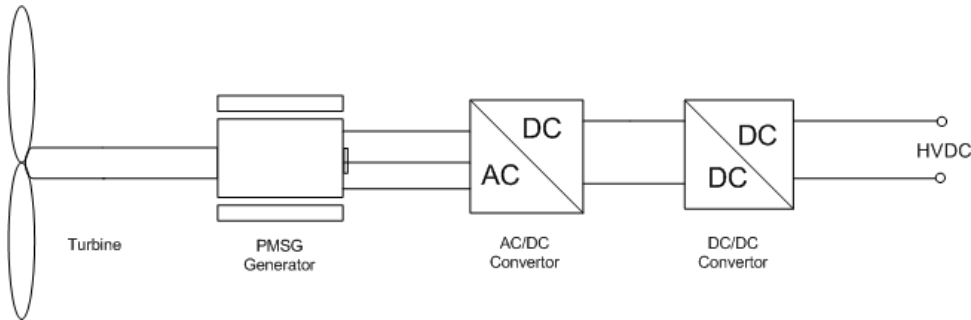
Fig. 3.1 System topology

The main idea to use the Vienna rectifier for this system instead of diode rectifier, as an AC/DC converter is a hope for better performance such as a higher output power and not increasing the losses too much.

.

The diode rectifier in this system can only produce 2.5 MW output power at a 4300 V dc-link voltage (it does not work on higher dc-link voltage) [2]. The generator that has been presented in [2], can operate with a transistor converter with 8400 V dc-link voltages and produce 5 MW. Therefore this type of converter does not have the same ability to control the output power, which could affect, its efficiency. Increased cost is the main disadvantage of using the Vienna rectifier in comparison with a diode rectifier. Due to the higher number of diodes and IGBTs cost will be increased in this type of converter.

3.2. PMSG Specification

As mentioned before, the generator that is used for this 5 MW wind turbine is a permanent magnet synchronous generator. It is assumed that permanent magnets established sinusoidal flux in stator that introduces sinusoidal electromotive force.
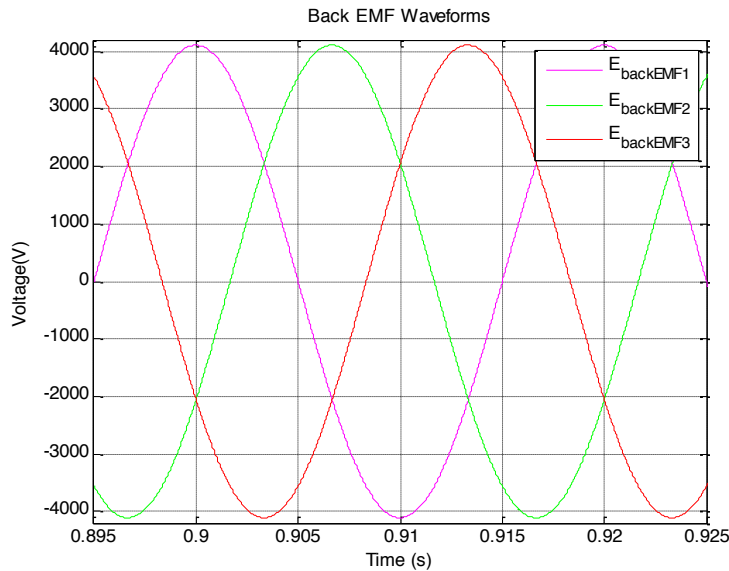

Fig. 3.2 Back EMF wave forms

Information and data regarding to the machine are given in Table 3.1.

Table 3.1 PMSG Data

Parameter	Value
Rated Output Power	5000(kW)
Rated Voltage	4800(V)
Frequency	50(Hz)
Fundamental Induced RMS Line Voltage	5032(V)
Stator Phase Resistance(R_s)	0.0374772(ohm)
Stator Phase Inductance(L_s)	15.3725(mH)
Flux Linkage	16.026(Vs)
Number of poles	8

3.3. Vienna rectifier set up

In a previous master thesis [2], a pure simple diode rectifier with a PMSG for a 5MW wind turbine was investigated. The goal with using a diode rectifier was to transfer a high rectified voltage to transmit power over long distance with low power losses. The transmitted power is a function of θ according to,

$$P = \frac{EV}{X} \sin \theta \tag{3.1}$$

where E is the back EMF, V is the phase voltage, X is reactance and θ angle between voltages.

Fig. 3.3 displays the maximum power that can be drawn from the generator with diode rectifier.
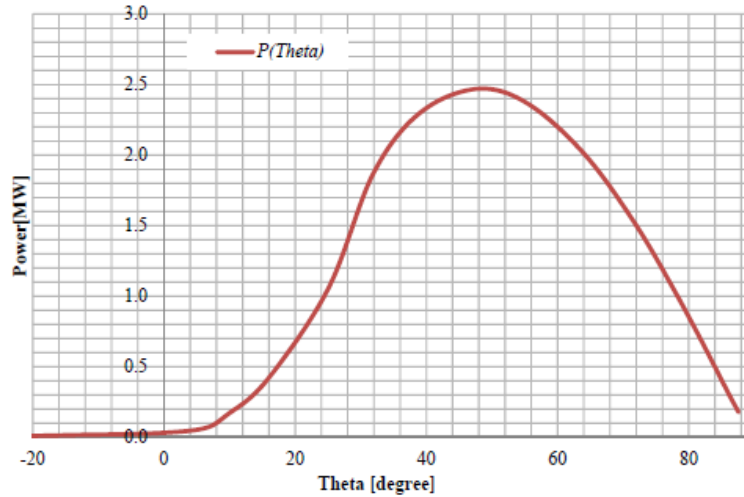

Fig. 3.3 Output power as function of θ, according to diode rectifier simulation at 4300 V dc-link voltage

It can be seen that at $\theta = 48°$, 2.5 MW can be extracted at 4300 V dc-link voltage [2].

In this thesis, the Vienna rectifier system is investigated and is designed based on the diode rectifier that could produce 2.5 MW output power.

As mentioned in Chapter 2, the Vienna rectifier consists of only three IGBTs. If all three switches are in the OFF state, the functionality is the same as for a diode rectifier and the output power result is exactly the same as for the diode rectifier (2.5 MW output power).

When switching of the IGBTs applied to the circuit, the Vienna rectifier is activated. The switches will operate with low switching frequency. In this application since we aim to obtain lower power loss, therefore there is only one switching for each half cycle. The IGBTs can turn-on at the beginning or at the end of the pulse, but since the phase voltage should lag the phase current, the switches are turned on at the beginning of the pulse. Fig. 3.4 explains switching pattern clearly.
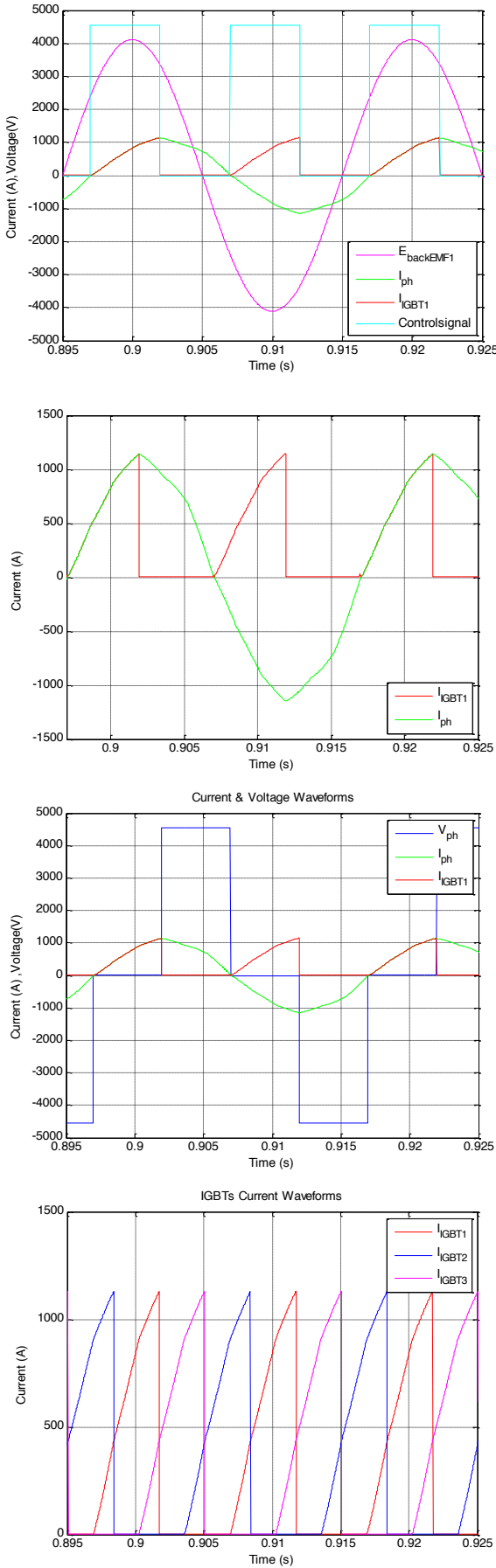
Fig. 3.4 Waveforms due to the IGBTs switching

3.4. Ideal Operating Point

According to (3.1) the output power of the converter depends on $''\theta''$ (angle between back EMF and phase voltage), therefore, in order to extract the maximum power; the best operating point for Vienna rectifier should be found.

Since the Vienna rectifier is to operate with a PMSG, this machine is modeled using dq-component theory as follows

$$u_{sd} = R_s\, i_{sd} - \omega_{el}\, L_q i_{sq} \tag{3.2}$$

$$u_{sq} = R_s\, i_{sq} - \omega_{el}\, L_d i_{sd} + \omega_{el}\, \psi_m \tag{3.3}$$

and the torque is formed as,

$$T_e = \frac{3}{2}\, P[\psi_m i_{sq} + (L_d - L_q) i_{sq}\, i_{sd}] \tag{3.4}$$

$$U_{phase\,(rms)} = \sqrt{\frac{u_{sd}^2 + u_{sq}^2}{2}} \tag{3.5}$$

$$I_{phase\,(rms)} = \sqrt{\frac{i_{sd}^2 + i_{sq}^2}{2}} \tag{3.6}$$

$$\varphi = \angle\, \vec{u_s} - \angle\, \vec{i_s} \tag{3.7}$$

This machine during normal PWM operation is controlled with maximum torque per ampere (MTPA) strategy to get the desired torque with minimum current and with a phase voltage and current limitation. When the voltage limit is reached, the machine is controlled with field weakening (extra voltage to provide torque when the rotor speed is increased) until the maximum current is reached [20].
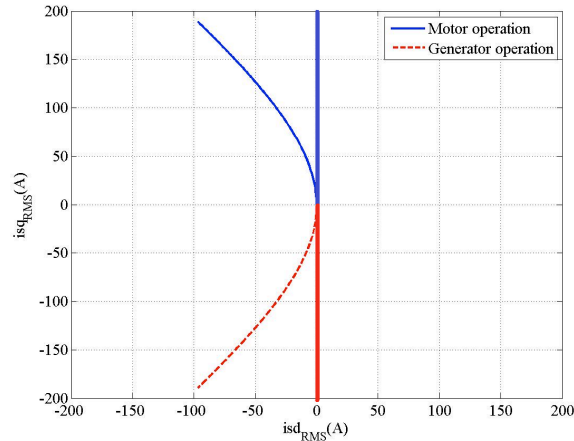
Fig. 3.5 MTPA current trajectory

Based on the PMSG model in dq-component form (3.2) to (3.7) and the machine parameters in Table 3.1, calculations are done for different cases to find a suitable angle.

The first case calculation is for a 5 MW with no d-axis current, the second case is for a 2.5 MW diode rectifier with 4300 V dc-link voltages. The result is shown in Table 3.2.

Table 3.2 Operating Point

			U(kV)	I(A)	$P_{converter}$(MW)
Case I	5MW	$i_{sd} = 0$ $i_{sq} = 813$	5.6∠ 46	813∠ 90	4.958
CaseII	2.5 MW	$i_{sd} = 430$ $i_{sq} = 407$	2.796∠ 45.69	592.071∠43.42	2.5

It is obvious that the voltage is lagging the current according to Table 3.2 (Case I) that is why the IGBT turns on at the beginning of the phase current in order to active this (see Fig. 3.4). Fig. 3.6 shows the operating point in all two cases.

It might be possible to control the Vienna rectifier with MTPA, since it is to some extent is an active rectifier and has the ability to control output AC-side voltage.
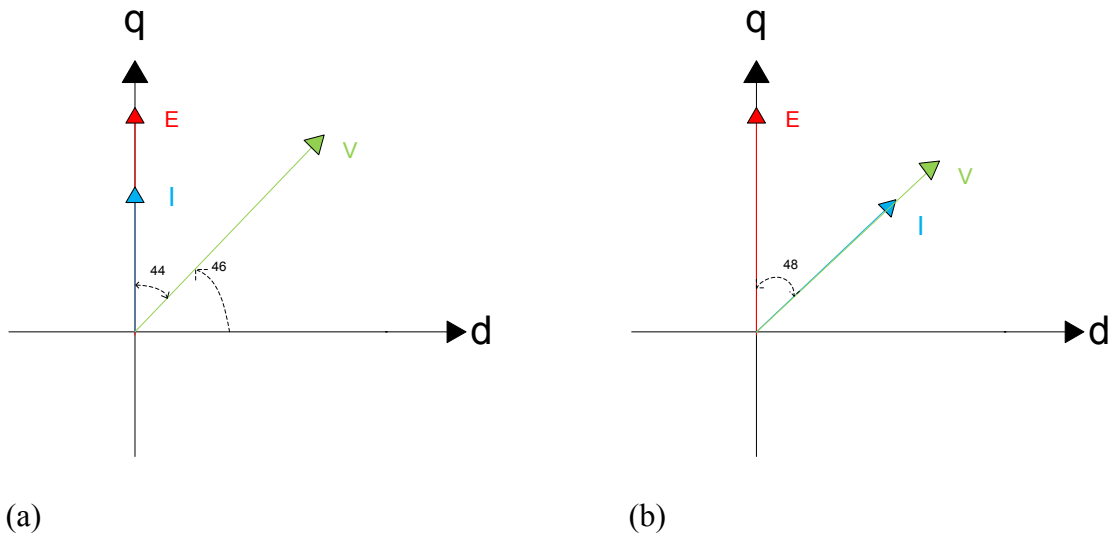
(a)   (b)

Fig. 3.6 Pharoses diagram of back EMF phase voltage phase current (a) case I (b) case II

In order to calculate the dc-link voltage, phase angle and other required parameters to find the best operating point for the Vienna rectifier, the transformation from Cartesian co-ordinations, to Polar co-ordinations, Fast Fourier analysis (FFT) has been used.

$$P = \frac{3}{2} E_{(1)} i_{(1)} cos\varphi \qquad (3.8)$$

As mention before, for the Vienna rectifier working with the PMSG the follow equations could be derived,

$$i_{(1)} = \frac{E - v_{(1)}}{R + j\omega L} \qquad (3.9)$$

By neglecting R in (3.9), the fundamental voltage can be determined.

Chapter 4

4. Analysis

The analysis and results in this thesis have been done by the help of two softwares; Ansys Simplorer and Matlab.

 MATLAB is a tool for technical and numerical computing and Ansys simplorer is multi domain simulation software and has a technology to model, simulate and analyze complicated circuits, especially in power electronic. It is a useful tool to evaluate interaction between components [21][22].

After that the Vienna rectifier has been simulated in Simplorer, all the results and data of the simulation is exported to Matlab and calculations have been done based on that.

This chapter includes different parts of the analysis; at first, accurate performance of the rectifier at different switching positions is investigated, and then the number of components that is required for the circuit is calculated. Thirdly, the loss calculation for the IGBT and Diode has been done. Moreover, the maximum power that can be extracted for this rectifier is calculated.

4.1 Analysis of Vienna Rectifier

As mentioned earlier, in this thesis the Vienna rectifier works with a PMSG. This machine provides sinusoidal flux in the stator. But in our simulation, instead of connecting the Vienna rectifier to the real machine, we provide sinusoidal voltage as an input for the rectifier.

It was mentioned in Chapter 3 that, the switches are turned on at the beginning of the pulse. When the IGBTs are conducting, the potential voltage becomes zero; otherwise the potential voltage is equal to $V_{dc}/2$. Fig. 4.1 shows it clearly.
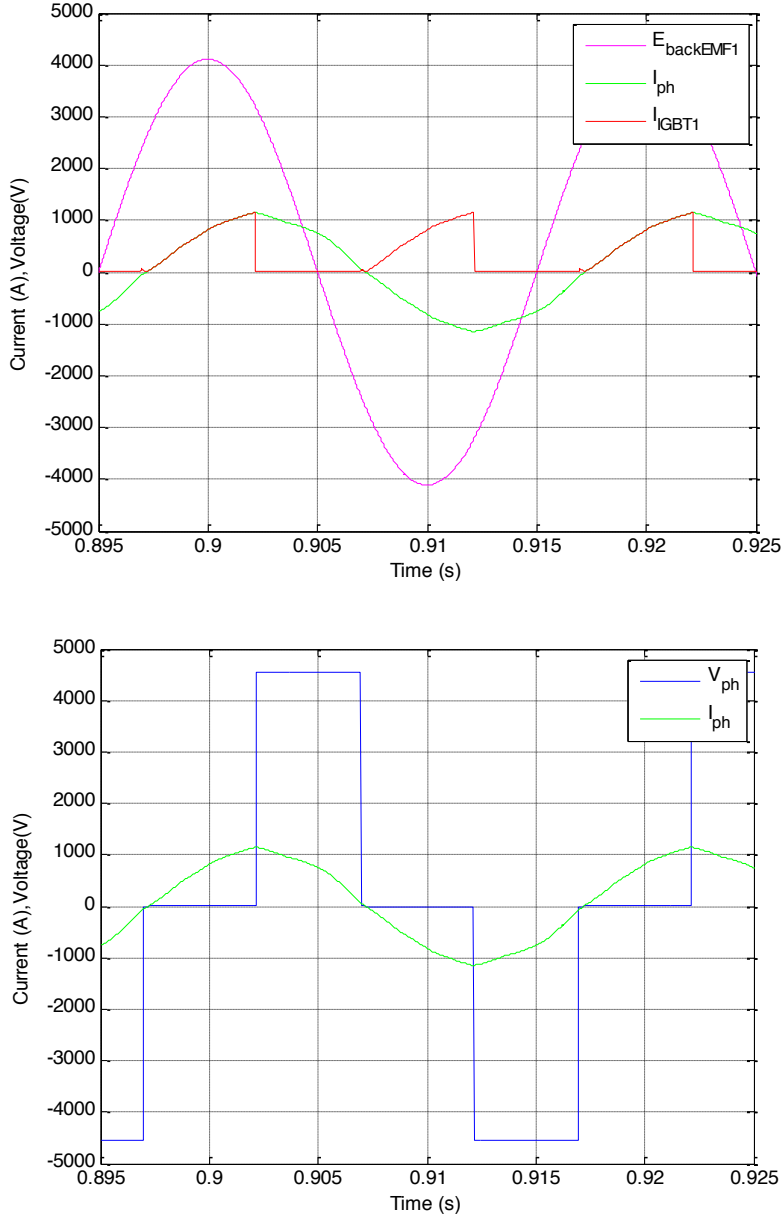
Fig. 4.1 Back EMF, phase current, IGBT current and potential voltage

The theory of the Vienna rectifier was explained in Chapter 2. There, it was described that the output voltage is a function of both switching state and current direction. The waveforms below that are taken from the simulation, confirmed this theory.
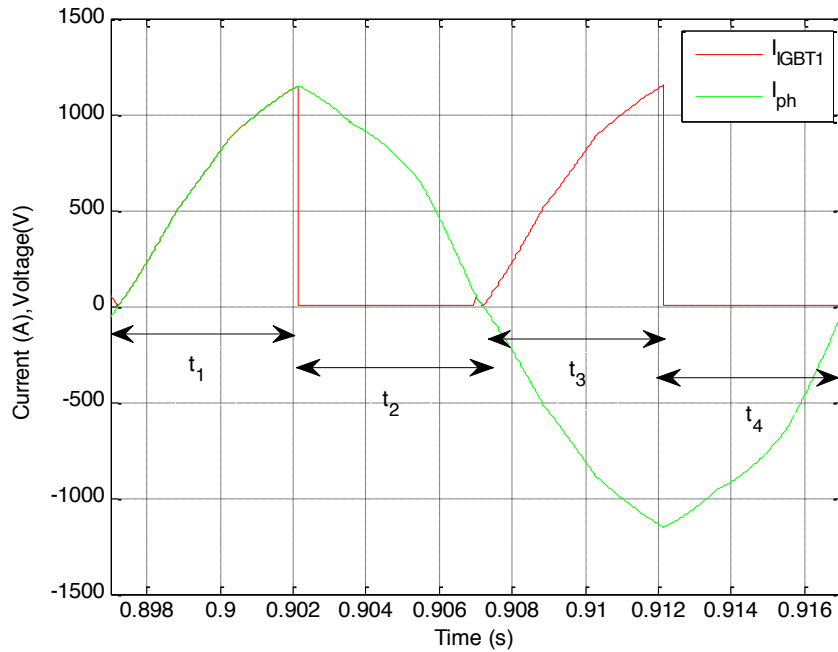
Fig. 4.2 Phase current and IGBT current for phase A

During time interval t_1, the IGBT is conducting, the phase current is positive, then current passes through D_{11} and D_{14}. Then, the phase potential voltage becomes zero.

During the time interval t_2, the IGBT is in its OFF state, and then the phase current passes through D_{11} and D_1. In this case, the phase potential voltage is equal to the positive dc-link voltage.

At t_3, the direction of the current is changed. While the IGBT is conducting, two diodes, D_{12} and D_{13}, are also conducting, and during t_4 the IGBT is not conducting, then both D_{12} and D_2 is a suitable path for the phase current and the potential voltage is equal to the negative dc-link voltage.
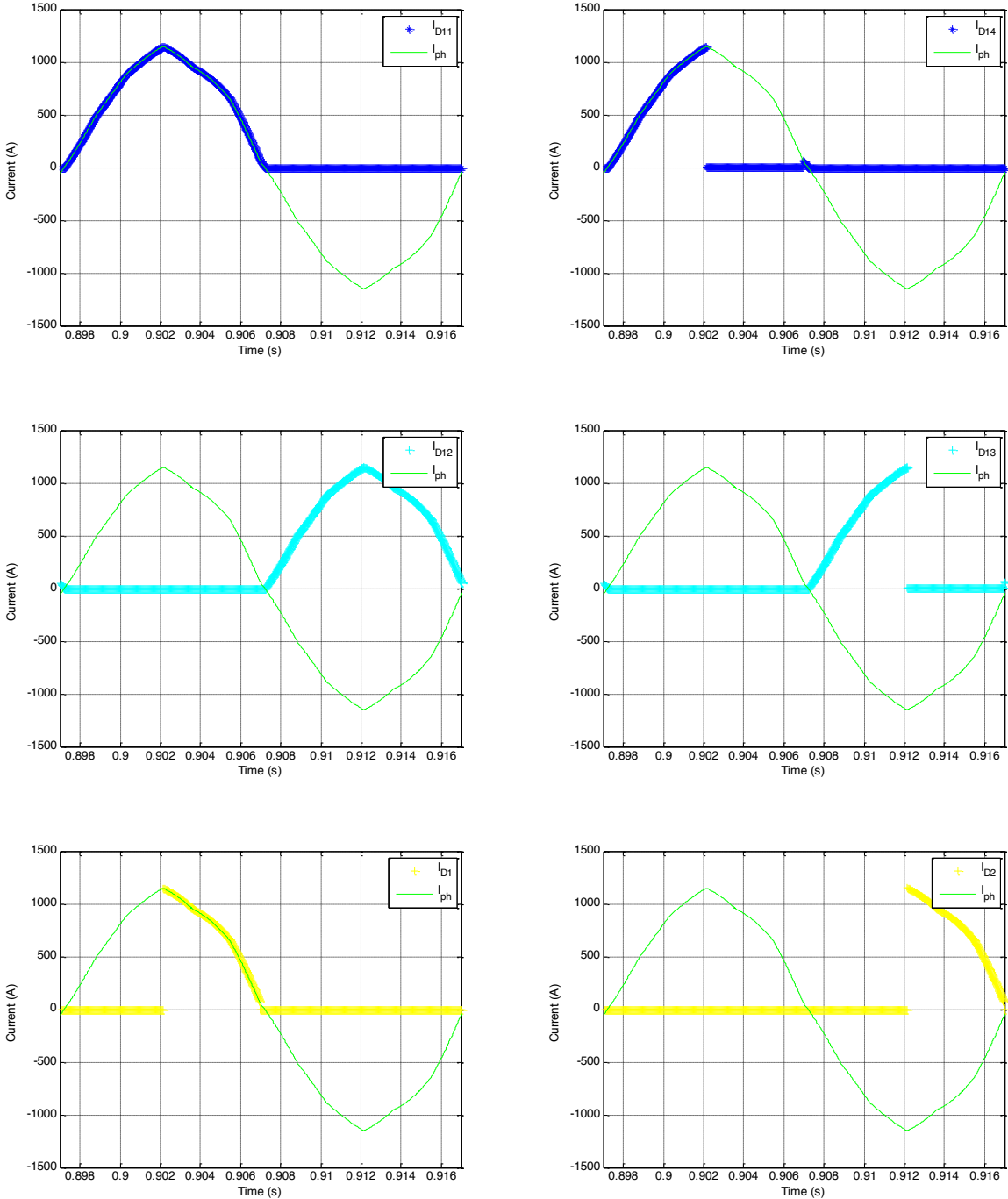
Fig. 4.3 Current path for phase A

Fig. 4.4 and Table 4.1 illustrate the phase potentials during one line period. These voltages depend on the switching state of the corresponding IGBT and the sign of the corresponding phase current.
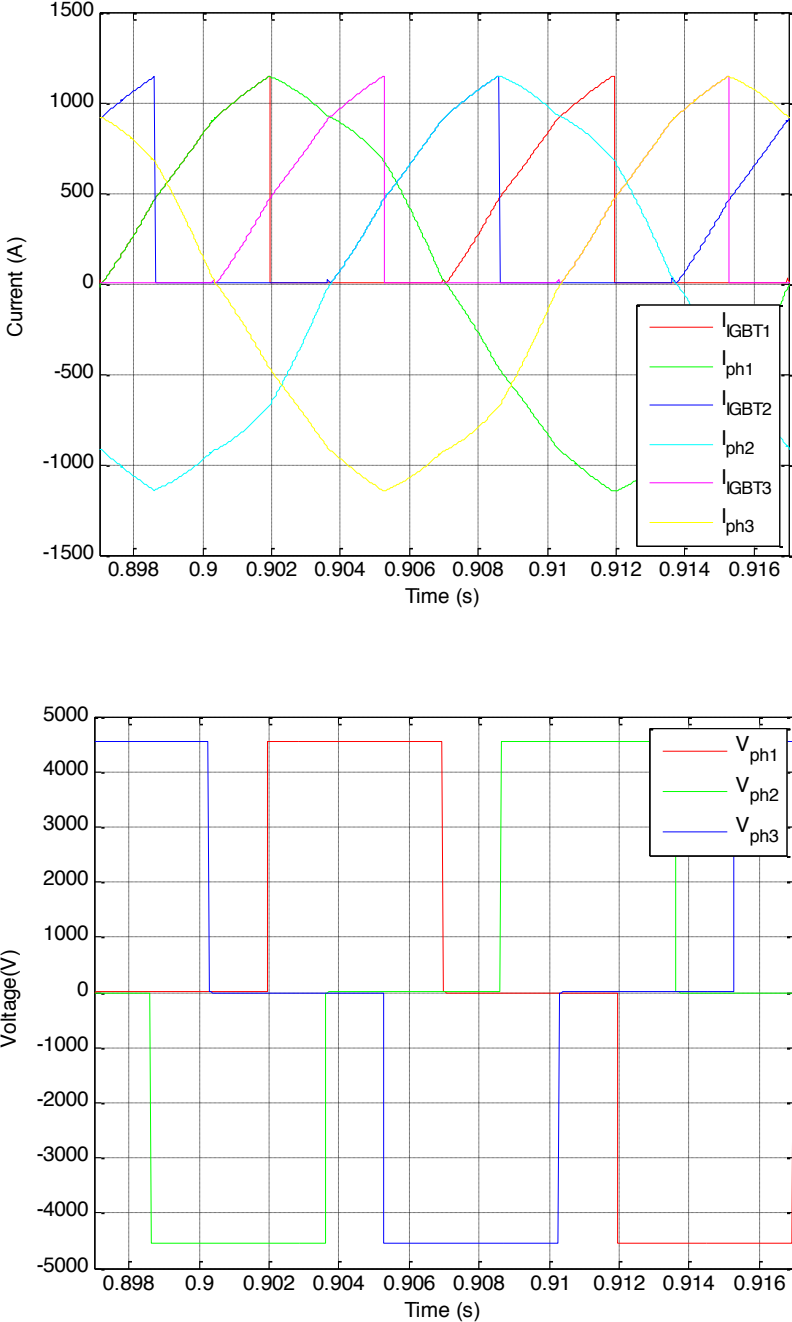

Fig. 4.4 The IGBTs current, the phase current and the phase potential voltage for three phase

Table 4.1 Input phase potentials

IGBT$_1$	IGBT$_2$	IGBT$_3$	V$_{1N}$	V$_{2N}$	V$_{3N}$
1	1	0	0	0	$+\dfrac{V_{dc}}{2}$
1	0	0	0	$-\dfrac{V_{dc}}{2}$	$+\dfrac{V_{dc}}{2}$
1	0	1	0	$-\dfrac{V_{dc}}{2}$	0
0	0	1	$+\dfrac{V_{dc}}{2}$	$-\dfrac{V_{dc}}{2}$	0
0	1	1	$+\dfrac{V_{dc}}{2}$	0	0
0	1	0	$+\dfrac{V_{dc}}{2}$	0	$-\dfrac{V_{dc}}{2}$
1	1	0	0	0	$-\dfrac{V_{dc}}{2}$
1	0	0	0	$+\dfrac{V_{dc}}{2}$	$-\dfrac{V_{dc}}{2}$
1	0	1	0	$+\dfrac{V_{dc}}{2}$	0
0	0	1	$-\dfrac{V_{dc}}{2}$	$+\dfrac{V_{dc}}{2}$	0
0	1	1	$-\dfrac{V_{dc}}{2}$	0	0
0	1	0	$-\dfrac{V_{dc}}{2}$	0	$+\dfrac{V_{dc}}{2}$

The space vector of the input phase potential is calculated as,

$$v = \frac{2}{3}\left(V_{1N} + \alpha V_{2N} + \alpha^2 V_{3N}\right) \tag{4.1}$$

where $= e^{j\frac{2\pi}{3}}$.

In the first half period, the voltage space vectors form a hexagon (A-B-C-D-E-F). For the next half period, this hexagon rotates counter-clockwise by $\frac{\pi}{3}$ (A-G-H-I-C-J).
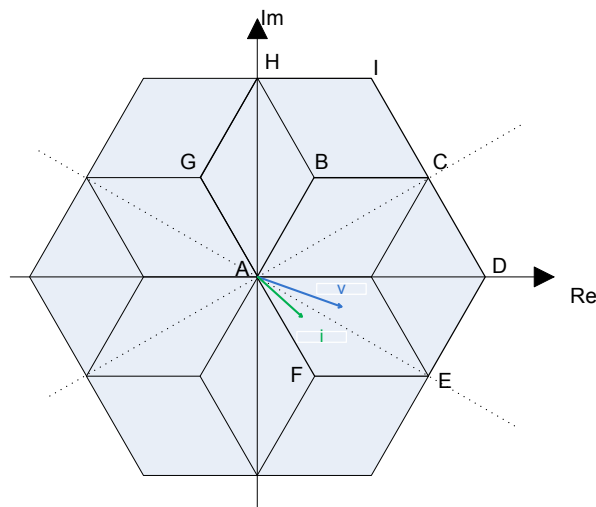

Fig. 4.5 Voltage space vectors of the Vienna rectifier input phase voltages

In [5] it is mentioned that, when the current space vector is located in intervals $\varphi \in (-\frac{\pi}{6}, \frac{\pi}{6})$, the possible voltage space vector must be located in the hexagon A-B-C-D-E-F. Therefore, the Vienna rectifier allows the input current to lead or lag the input voltage by no more than 30°. However, the simulations have not verified that results. As will describe further, the maximum possible extracted output power for this generator is when the phase shift between voltage and current is around 43°.

4.2 Component Selection

4.2.1 IGBT Selection

The maximum voltage across each IGBT is equal to 4550 V; this voltage is half of the dc-link voltage. The maximum current when it is conducting is equal to 1150 A; while the rms current is equal to 518 A. Based on this characteristic, an IGBT module of 4.5 kV 1200 A [17] is selected. However, in order to fulfill the maximum current and voltage for each switch, the number of this module should be connected to each other, in series or parallel.

The relation between I_{ref} and $I_{rated\ (rms)}$ is approximately,

$$I_{rated(rms)} = \frac{I_{ref}}{2} = \frac{1200}{2} = 600 \tag{4.2}$$

so, the number of module in parallel is,

$$n_{parallel} = \frac{max|I_{rms}|}{I_{rated(rms)}} = \frac{518}{600} = 0.86 \tag{4.3}$$

and the needed number of modules in series can found as,

$$n_{series} = \frac{V_{dc}}{V_{ref}} = \frac{4550}{2800} = 1.625 \tag{4.4}$$

where I_{ref} module reference current, V_{ref} module reference voltage. (Usually little bit more than half the rated module voltages.)

4.2.2 Diode Selection

According to simulation, the maximum voltage across the diode is 4550 V, but each diode has the specific rms current value due to different conduction path, e.g. rms currents for D_1 and D_2 are 405 A, D_{11} and D_{12} are 550 A; D_{13} and D_{14} are 365 A. Based on these values the diode module of 6500V, 2*600 A [18] is selected.

A number of this module should be connected together in series or in parallel to fulfill the required voltage and current for diode.

$$I_{rated(rms)} = \frac{I_{ref}}{2} = \frac{600}{2} = 300 \tag{4.5}$$

the number of module in parallel is,

$$n_{parallel} = \frac{max|I_{rms}|}{I_{rated(rms)}} = \frac{550}{300} = 1.83 \tag{4.6}$$

Since the selected module has two diodes, one module is enough. And the needed number of modules in series can found as,

$$n_{series} = \frac{V_{dc}}{V_{ref}} = \frac{4550}{3600} = 1.26 \tag{4.7}$$

The maximum current, rms current and average current for the IGBT$_1$ and the D$_1$ are shown in Fig. 4.5, during one line period.

(a)

(b)
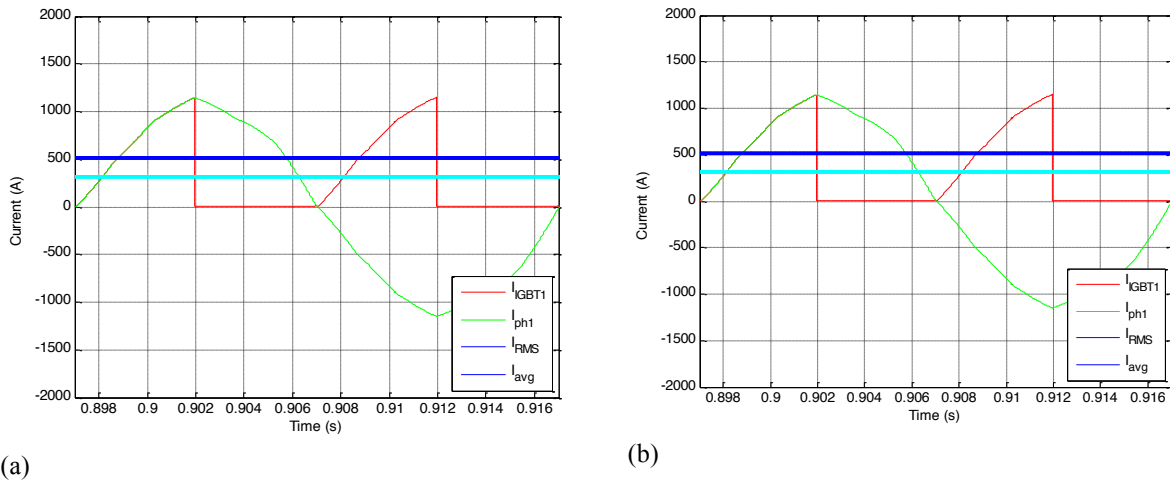
Fig. 4.6 (a) IGBT current (b) Diode current (D$_1$)

4.3 Power Loss Calculation

In this section, the conduction and the switching loss calculation for both the IGBT and the diode is investigated. (It is assumed that the temperature is 125^{oc} for all calculations).

Fig. 4.6 shows the switching characteristics.
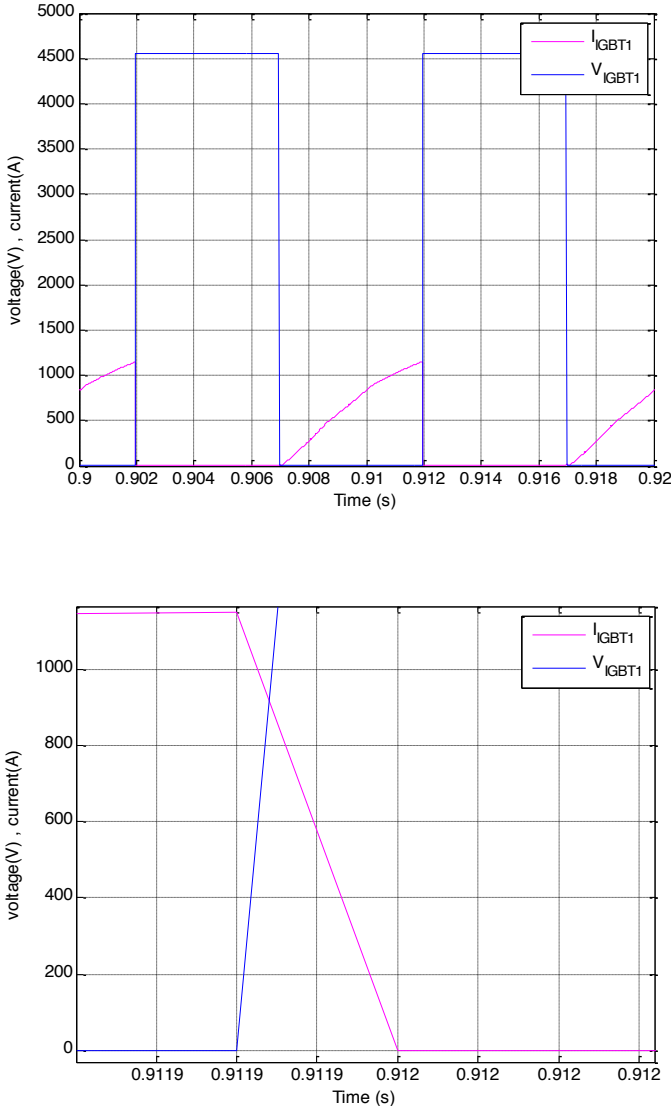
Turn-off switching

Fig. 4.7 IGBT current and voltage wave form

As Fig. 4.6 shows, the IGBT turns-on only twice during one line period and it conducts for 90° (Duty cycle =0.5) during half the period.

According to Chapter 2, the conduction losses are calculated by using the forward voltage drop and on-state current, as well as on-state resistance according to (2.11) and Fig. 4.6.
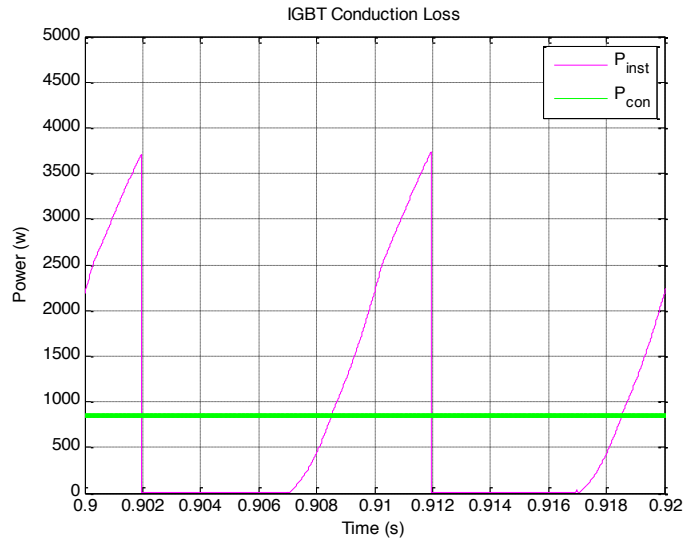
Fig. 4.8 IGBT conduction loss,

Turn-on loss can be neglected and the switching loss only consists of turn-off switching loss.

According to (2.16) to (2.18), the conduction loss and switching loss for each component is calculated separately. Table 4.2 shows the results.
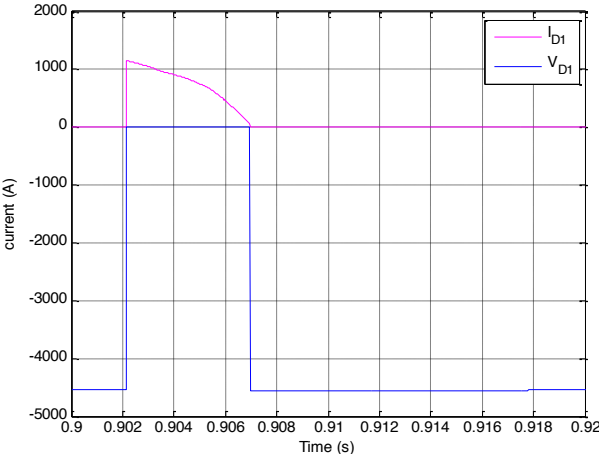
Table 4.2 loss for leg A

	P_{cond} (w)	$P_{sw(on)}(w)$	$P_{sw(off)}(w)$	P_{sw} (w)	P_{Loss} (w)
IGBT$_1$	889.5635	43.357	1014.7	1058.1	1947.7
D$_1$	556.46	-	-	81.45	637.92
D$_{11}$	1050.7	-	-	0	1050.7
D$_{12}$	1043.6	-	-	0	1043.6
D$_{13}$	494.24	-	-	81.30	575.54
D$_{14}$	494.18	-	-	81.45	575.63
D$_2$	549.29	-	-	81.30	630.59
Total loss for one leg					6461.7

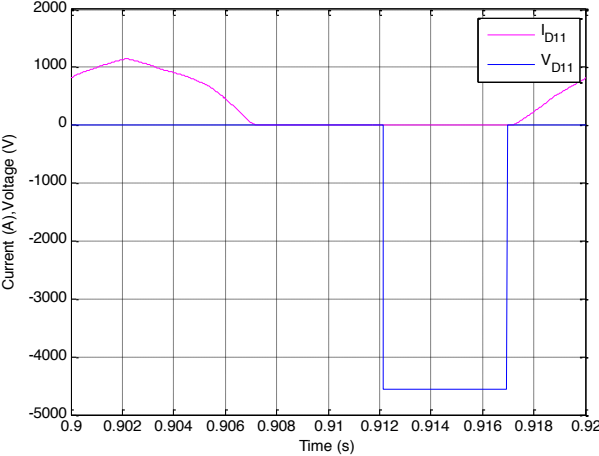Fig. 4.8 shows conduction and switching losses for each component during the one period.
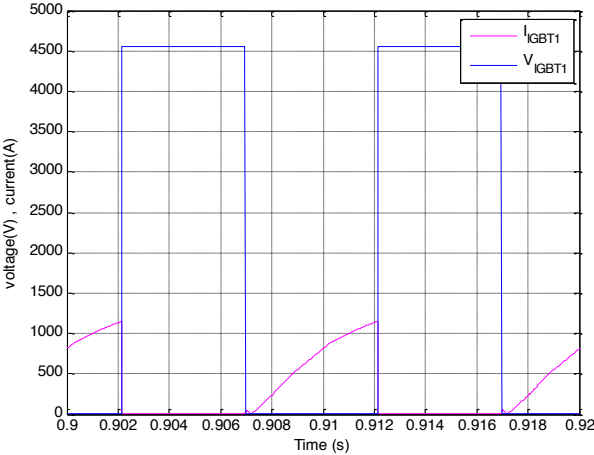
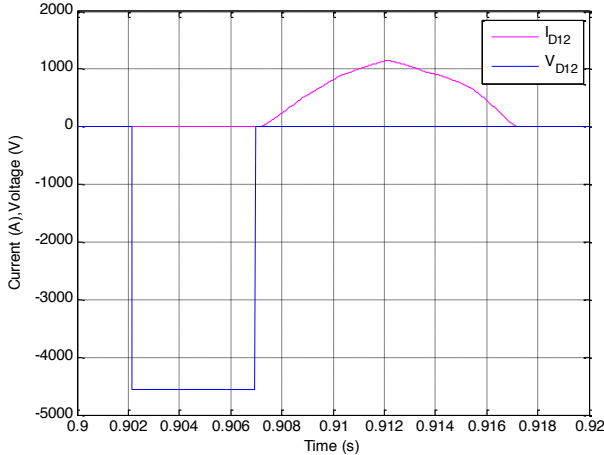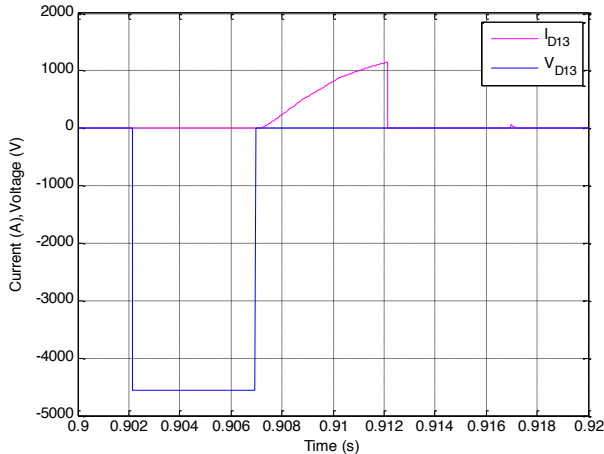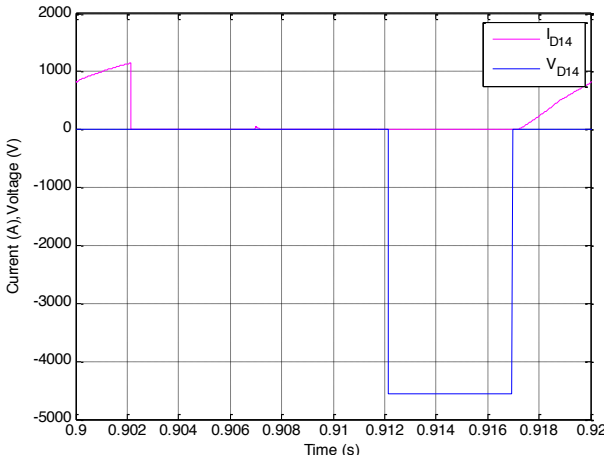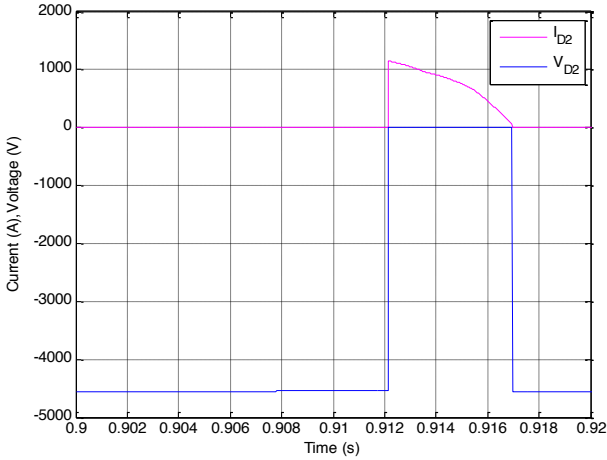(a)

(b)

(c)

(d)

(e)

(f)

(g)

Fig. 4.9 IGBT and diode switching (a) IGBT$_1$ (b) D$_1$, (c) D$_{11}$, (d) D$_{12}$, (e) D$_{13}$, (f) D$_{14}$, (g) D$_2$

4.4 Output Power Calculation

Output power of rectifier is calculated based on the following relations,

$$P = \frac{3}{2} \left| u_{(1)} \right| . \left| i_{(1)} \right| . \cos \varphi \tag{4.8}$$

$$Q = \frac{3}{2} \left| u_{(1)} \right| . \left| i_{(1)} \right| . \sin \varphi \tag{4.9}$$

$$S = \sqrt{P^2 + Q^2} \tag{4.10}$$

In Chapter 3, the minimum dc-link voltage was calculated. Also an effort is made to extract 5 MW output power. The simulation shows that at 9100 V dc-link voltage the extracted output power is equal to 5 MW by 43° phase shift.

Table 4.3 shows the results for different conduction intervals for the IGBTs.

Table 4.3 Output power for a dc-link voltage 9100 V

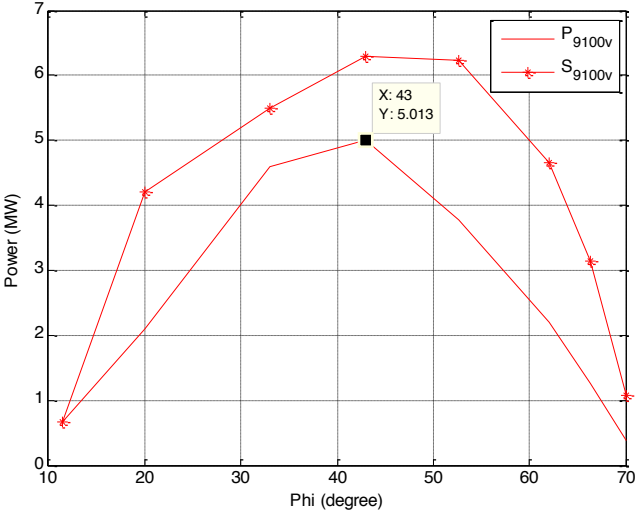| IGBT conducts for	V_{ph}(V)	I_{ph}(A)	φ	P_{output}(MW)	S(MW)
36°	3964	113	11.4	0.67	0.67
72°	4580	804	33	4.6	5.5
90°	3968	1150	43	5.013	6.3
108°	3258	1277	52.6	3.77	6.24
126°	2468	1263	62	2.2	4.66
144°	1792	1175	66.3	1.26	3.15
162°	727	991	70	0.385	1.07

Fig. 4.10 Output power and apparent power for a dc-link voltage 9100 V

As mentioned before, one of the Vienna rectifier's characteristics is that it can work in a wide voltage range. So, in order to be able to compare with the diode rectifier and conventional IGBT converter the operation of the Vienna rectifier is evaluated at 4300 V and 8400 V dc-link voltages. The results are shown in Table 4.4 and 4.5.

Table 4.4 Output power for a dc-link voltage 8400V

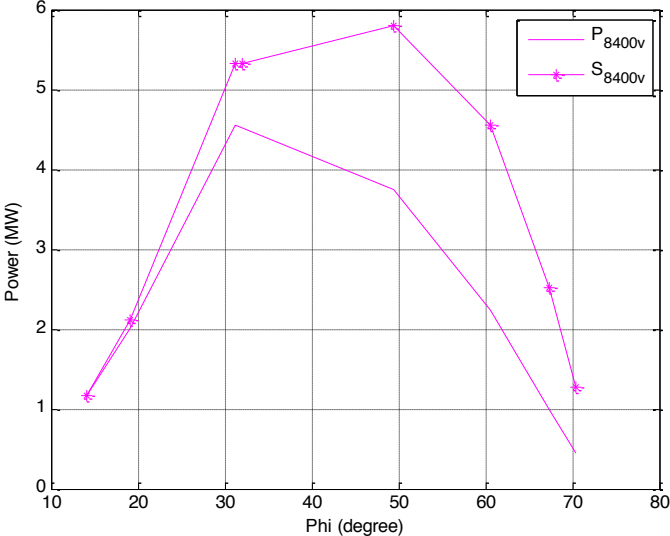| IGBT conducts for	$V_{ph}(V)$	$I_{ph}(A)$	φ	$P_{output}(MW)$	S(MW)
36°	4237	183	14.12	1.16	1.16
54°	4325	326	19.1	2.01	2.11
72°	4329	820	31.18	4.55	5.32
90°	3784	938	32.	4.51	5.32
108°	3146	1228	49.4	3.75	5.79
126°	2430	1248	60.53	2.24	4.55
144°	1493	1126	67.39	0.985	2.52
162°	838	1011	70.35	0.446	1.27

Fig. 4.11 Output power and apparent power for a dc-link voltage 8400 V

Table 4.5 Output power for a dc-link voltage 4300V

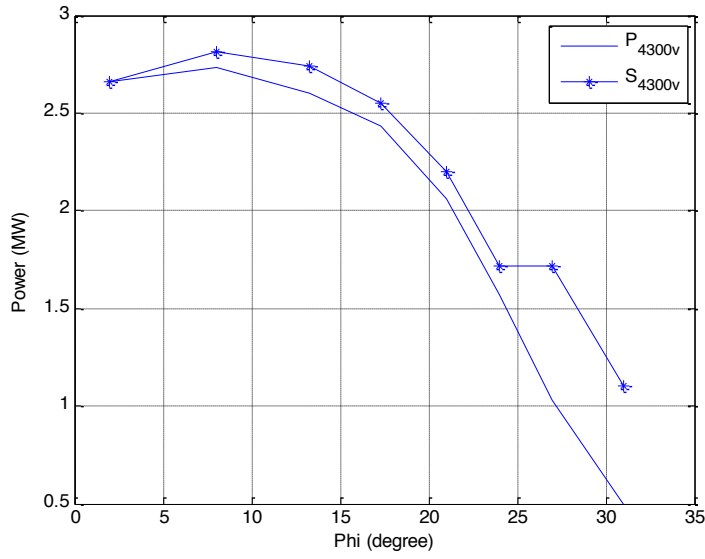| IGBT conducts for	$V_{ph}(V)$	$I_{ph}(A)$	φ	$P_{output}(MW)$	S(MW)
36°	2606	681	2	2.66	2.66
54°	2441	760	8	2.73	2.81
72°	2217	826	13.25	2.6	2.74
90°	1938	878	17.32	2.43	2.55
108°	1612	911	21	2.06	2.2
126°	1245	925	24	1.57	1.72
144°	848	920	27	1.03	1.17
162°	430	897	31	0.5	0.57

Fig. 4.12 Output power and apparent power for a dc-link voltage 4300 V

Fig. 4.13 shows the power diagram at three different dc-link voltages.
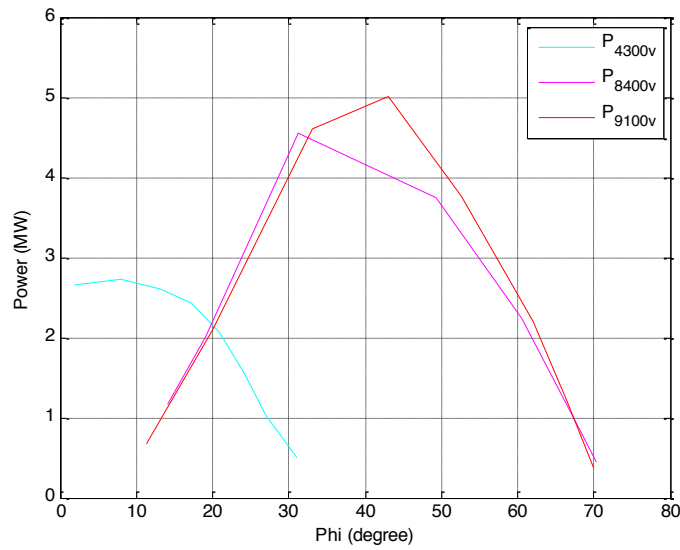

Fig. 4.13 Output power and apparent power for the different dc-link voltages

4.5 The Vienna Rectifier vs the Diode Rectifier

In the previous thesis [2], the diode rectifier in a 5MW wind turbine has been investigated. The maximum transmitted power of the PMSG connected to the diode rectifier is 2.5 MW at

4300 V dc-link voltage. In order to extract 5 MW power form this generator, series and shunt compensation are examined. By using a series capacitor, the imaginary part of the impedance of the generator is reduced and the transmittable power is increased. Shunt compensation is also another way to increase the output power of the system. However, it is not as effective as series compensation for increasing the capability of the power transmission. Fig. 4.14 shows these two different compensations.
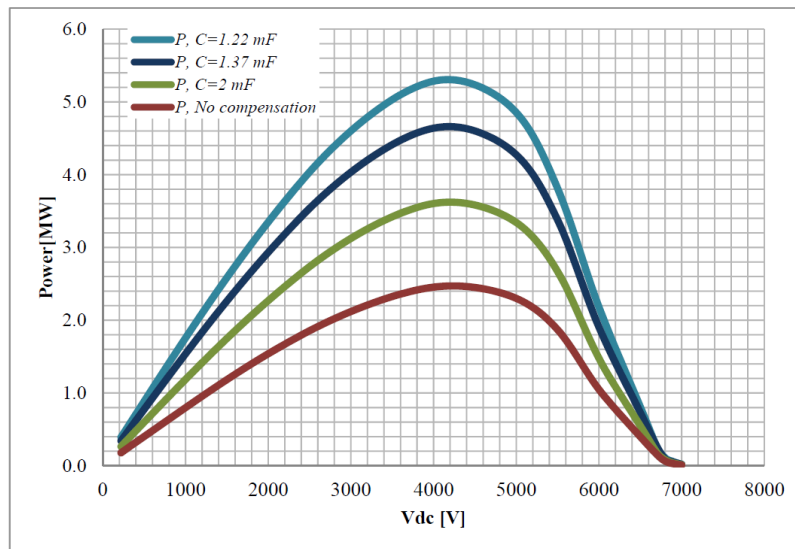
(a)
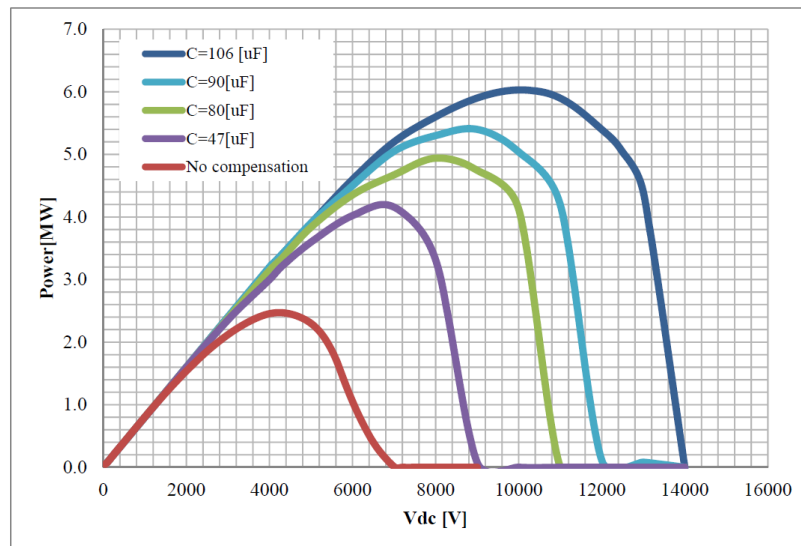
(b)

Fig. 4.14 Output power with and without compensation (a)series compensation (b)shunt compensation for the PMSG connected to the diode rectifier

Fig. 4.15 illustrates the operation of the Vienna rectifier at different dc-link voltages. As described before, the Vienna rectifier has an ability to operate on a wide range of dc link voltages

The results show that there is a possibility to extract 5 MW output power from the system at 9100 V dc where there is no need for compensation.
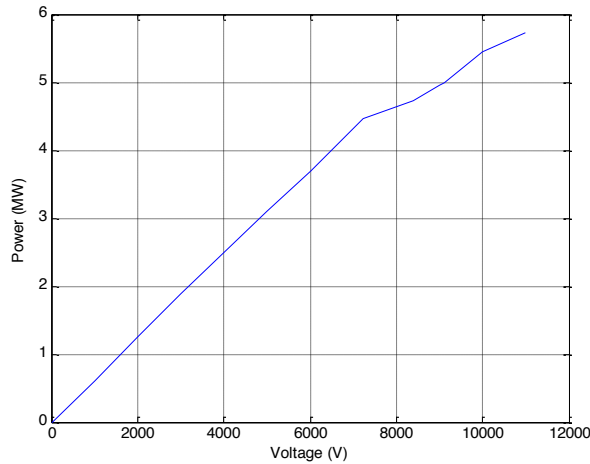

Fig. 4.15 Output power at different dc-link voltages for the PMSG connected to the Vienna rectifier

4.6 Output capacitor size

The aim of this part is to calculate the size of the output capacitors for the Vienna rectifier. At first, it is assumed that the limitation for the output voltage ripple is 5%. Therefore the maximum voltage across the each capacitor is 4673. By simple calculation the capacitors value can be found.

$$u = \frac{1}{C} \int i \, dt \qquad (4.11)$$

According to the assumption and (4.11) the calculated value for capacitors is 117 mF, which is very high value. Therefore, instead of using the capacitors with high capacity and high cost, power batteries are suggested. This is justified by the fact that switching occurs rather seldom. Fig 4.16 shows the waveform for the output current and the capacitor voltage.
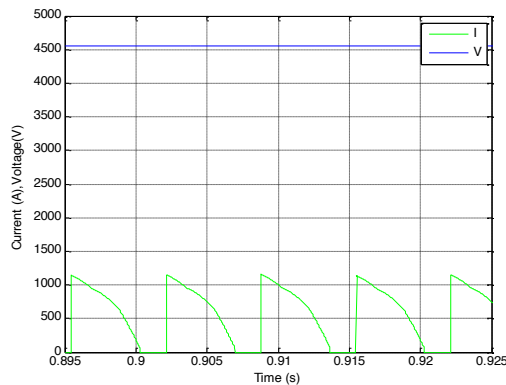

Fig. 4.16 The output current and the capacitor voltage the Vienna rectifier

Chapter 5

5. Conclusion

5.1. Result From Present Work

In this thesis, it is shown and explained how it is possible to use a Vienna rectifier for a 5 MW PMSG system in a wind turbine system to be connected to an HVDC grid. The system is simulated in the Ansys Simplorer software and calculations have been done by Matlab.

In Chapter 3, the Vienna rectifier setup with a PMSG has been explained and the analytical relation between electrical power and dc-link voltage has been proposed.

It can be seen from the simulation in Chapter 4, that the Vienna rectifier has low losses due to a very low switching frequency. The IGBTs are turned-on only twice during the one line period. It also has been shown that, the output power that can be extracted is 5 MW with a 43° phase shift angle. This power is extracted when the output dc-link voltage has the value, 9100 V. Simulations have also performed for two different dc-link voltages, 4300 V, 8400 V. The results show that the maximum output power at 4300 V dc-link voltage is 2.7 MW and at 8400 V is 4.55 MW.

The results show that the Vienna rectifier has higher efficiency in comparison with the conventional IGBT converter and lower efficiency in comparison with the diode rectifier. The pure diode rectifier that works with the same generator can only provide 2.5 MW and the conventional IGBT converter provides 5MW output power.

5.2. Future work

The main focus of this thesis has been on the behavior of the Vienna rectifier with a PMSG for a 5 MW wind turbine system. The Vienna rectifier has been simulated in the Simplorer software with a low switching frequency. It might be interesting to design a real PMSG and connect the Vienna rectifier to it.

It could be interesting to extend this thesis by designing an output filter and connect the Vienna rectifier to the DC/DC converter.

In this work, only the losses in the switches are considered, that could be a continuing this work, to investigate the losses in the cables and the thermal calculation in the rectifier.

It is also possible to study the control topology for the Vienna rectifier with a PMSG.

Finally, a cost evaluation for system could be achieved and the result could be compared with the diode rectifier and the conventional IGBT converter.

References

[1] "Wkipedia " [Online]. Available: http://en.wikipedia.org/wiki/Wind_power [Accessed 11 May 2013]

[2] A. Mazaheri," A 5 MW Wind Turbine Generator System for a DC Grid Application", Master thesis, Dept. Energy& Environment, Chalmers University of Technology, Gothenburg, Sweden, 2012

[3] F. Blaabjerg, M. Liserre, K. Ma, "Power Electronic Converters For Wind Turbine", Industry applications, Vol. 48, No. 2, March/April 2012.

[4] S. Heier, "Grid Integration of Wind Energy Conversion System", 2nded. Chichester, England; Hoboken, NJ: Wiley, 2006.

[5] H.Chen, D.C. Aliprantis," Induction Generator With Vienna Rectifier: Feasibility Study For Wind Power Generation", .XIX international conference on electric Machines-ICEM, Rome, 2010.

[6] O. Carlson," Sustainable Power Production And Transportation", Chalmers University of Technology, Gothenburg, Sweden, 2011.

[7] A. H. Rajaei, M. Mohamadian, S. M. Dehghan, A. Yazdian," PMSG-Based Variable Speed Wind Energy Conversion System Using Vienna Rectifier", Euro. Trans. Electr. Power 2011; 21:954-972.

[8] "PMSG"[Online]. Available:http://en.wikipedia.org/wiki/Permanent_magnet_synchronous_generator [Accesses 25 April2013]

[9] R. Melício, V.M. F. Mendes and J. P. S. Catalão," Wind Turbines with Permanent Magnet Synchronous Generator and Full-Power Converters: Modeling, Control and Simulation" [on line], Available: http://www.intechopen.com/.[Accesses 5 April2013]

[10] Johann W. Kolar, "IEEE power Electronic society" [Online]. Available: http: // www. ieee-pels.org/chapters/distinguished-lecturers/110-products/webinars/800-johann-w-kolar Johann. [Accesses 10 Feb 2013]

[11] Dr. T. Govindaaji, "Analysis of Vienna Rectifier for DC Drive", Muthayammal Engineering college, India, 2012.

[12] H.Chen, D.C. Aliprantis, " Analysis Of Squirrel-Cage Induction Generator With Vienna Rectifier For Wind Energy Conversion System", IEEE Transaction on energy conversion, Vol. 26, No.3, 2011.

[13]   G. Radomski, "Voltage Space Vector Control System of Vienna Rectifier I", Technical university of Kielce, Poland, international Conference, Eurocon,2012.

[14]   L. He, X. Chen," A Neutral Point Potential Balance Control Strategy Based on Vector Controlled Vienna Rectifier", IEEE,978-1-4244-5287-3/10,2010.

[15]   A.D. Pathak, R. E. Locher, H.S.Mazumdar,"3-Phase Power Factor Correction, Using Vienna Rectifier Approach and Modular Construction For Improved Overall Performance, Efficiency and Reliability", Power electronics Conference, CA, USA, 2003.

[16]   G.Radomski, "Analysis of Vienna Rectifier", Technical university of Kielce, Poland, Electrical power quality and utilization, Journal Vol.XI, No.1, 2005.

[17]   ABB HiPak and IGBT Module,"5SNA 01200G450300", ABB Switzerland Ltd, 2009.

[18]   ABB HiPak and Diode Module,"5SLD 0600J650100", ABB Switzerland Ltd, 2010.

[19]   Semikron,"Theory of loss and Temperature Calculation", 2008 [Online] Available: http://www.semikron.com/skcompub/en/eng_3_2_1_3.pdf.

[20]   O. Josefsson, Energy Efficiency Comparison Between Two-level and multilevel Inverters for Electric Vehicle Applications, Licentiate thesis, Dept. Energy& Environment, Chalmers University of Technology, Gothenburg, Sweden (2013)

[21]   "Mathwork", [On line]. Available: http://www.Mathworks.se/help/toolbox/physmod/ powersys/ref/igbt.html. [Accesses 15 May2013]

[22]   "ANSYS",[Online].Available:http://www.ansys.com/products simulation+Technology/Electromagnetics/Electromechanical+Design/ANSYS+simplo rer.[Accesses15May2013]

[23]   N.Mohan, T.M. Undeland and W.P. Robbins, "Power Electronics Converters, Applications and Design "

[24]   "APPLYING IGBTs",[Online].Available: http://www05.abb.com/global/scot/ApplyingIGBTs.pdfrer. [Accesses12Feb2013]

Apendix

Machine Data(PMSG)

GENERAL DATA			
Rated Output Power (kW)	5000	Frictional Loss (W)	0
Rated Voltage (V)	4800	Windage Loss (W)	0
Number of Poles	8	Rotor Position	Inner
Frequency (Hz)	50	Operating Temperature (C)	75

STATOR DATA			
Number of Stator Slots	24	Number of Conductors per Slot:	44
Outer Diameter of Stator (mm)	1100	Average Coil Pitch	2
Inner Diameter of Stator (mm)	757.9	Number of Wires per Conductor	1
Top Tooth Width (mm)	59.9173	Wire Diameter (mm)	9.266
Bottom Tooth Width (mm)	53.6687	Slot Area (mm^2)	6759.14
Skew Width (Number of Slots)	0	Net Slot Area (mm^2)	6190.79
Length of Stator Core (mm)	945	Stator Slot Fill Factor (%)	61.0227
Stacking Factor of Stator Core	0.95	Coil Half-Turn Length (mm)	1323.43
Number of Parallel Branches	2		

ROTOR DATA			
Minimum Air Gap (mm)	3	Electrical Pole Embrace	0.596409
Inner Diameter (mm)	400.4	Max. Thickness of Magnet (mm):	28
Length of Rotor (mm)	945	Width of Magnet (mm)	197.067
Stacking Factor of Iron Core	0.95	Type of Magnet:	NdFe30
Polar Arc Radius (mm)	195.95	Magnetic Shaft:	No
Mechanical Pole Embrace	0.7		

PERMANENT MAGNET DATA			
Residual Flux Density (Tesla)	1.1	Demagnetized Flux Density (Tesla)	0.647015
Coercive Force (kA/m)	838	Recoil Residual Flux Density (Tesla)	1.1
Maximum Energy Density (kJ/m^3)	230.45	Recoil Coercive Force (kA/m)	838
Relative Recoil Permeability	1.0446		

MATERIAL CONSUMPTION			
Armature Copper Density (kg/m^3)	8900	Armature Core Steel Weight (kg)	2329.36
Permanent Magnet Density (kg/m^3)	7550	Rotor Core Steel Weight (kg)	1758.83
Armature Core Steel Density (kg/m^3)	7700	Total Net Weight (kg)	5198.06
Rotor Core Steel Density (kg/m^3)	7700	Armature Core Steel Consumption (kg)	8410.02
Armature Copper Weight (kg)	838.741	Rotor Core Steel Consumption (kg)	3376.57
Permanent Magnet Weight (kg)	271.133		

STEADY STATE PARAMETERS			
Stator Winding Factor	0.866025	Armature Leakage Reactance X1 (ohm)	1.90086
D-Axis Reactive Reactance Xad (ohm)	2.92968	Zero-Sequence Reactance X0 (ohm)	0.394111
Q-Axis Reactive Reactance Xaq (ohm)	2.92968	Armature Phase Resistance R1 (ohm)	0.0374772
D-Axis Reactance X1+Xad (ohm)	4.83054	Armature Phase Resistance at 20C (ohm)	0.030828
Q-Axis Reactance X1+Xaq (ohm)	4.83054		

NO-LOAD MAGNETIC DATA			
Stator-Teeth Flux Density (Tesla)	1.78945	Magnet Flux Density (Tesla)	0.87569
Stator-Yoke Flux Density (Tesla)	1.64989	Fundamental Induced RMS Line Voltage (V)	5032.09
Rotor-Yoke Flux Density (Tesla)	0.614729	THD of Induced Voltage (%):	11.0593
Air-Gap Flux Density (Tesla)	0.966052	Cogging Torque (N.m)	177.89

FULL-LOAD DATA			
RMS Line Current (A)	742.962	Output Power (MW)	5.00152
RMS Phase Current (A)	742.962	Input Power (MW)	5.07346
RMS Phase Voltage (V)	2771.18	Efficiency (%)	98.5819
Armature Thermal Load(A^2/mm^3)	90.7613	Apparent Power (MVA):	6.17663
Specific Electric Loading (A/mm)	16.4755	Power Factor	0.809748
Armature Current Density (A/mm^2)	5.50886	Synchronous Speed (rpm)	750
Frictional and Windage Loss (W)	0	Rated Torque (N.m)	64597.3
Iron-Core Loss (W)	9883.42	Power Angle (degree)	70.0171
Armature Copper Loss (W):	62061.4	Maximum Output Power (MW)	5.31863
Total Loss (W)	71944.8	Short Circuit Current (A)	641.93

TRANSIENT FEA INPUT DATA			
For Armature Winding		2D Equivalent Value	
Number of Turns	176	Equivalent Model Depth (mm)	945
Parallel Branches	2	Equivalent Stator Stacking Factor	0.95
Terminal Resistance (ohm)	0.0374772	Equivalent Rotor Stacking Factor	0.95
End Leakage Inductance (H)	0.000393811	Equivalent Br (Tesla)	1.1
		Equivalent Hc (kA/m)	838
		Estimated Rotor Inertia (kg m^2)	231.295

V_{RRM} = 6500 V
I_F = 2x 600 A

ABB HiPak[TM]

DIODE Module
5SLD 0600J650100

- **Low-loss, rugged SPT diode**
- **Smooth switching SPT diode for good EMC**
- **Industry standard package**
- **High power density**
- **AlSiC base-plate for high power cycling capability**
- **AlN substrate for low thermal resistance**

Maximum rated values [1]

Parameter	Symbol	Conditions	min	max	Unit
Repetitive peak reverse voltage	V_{RRM}			6500	V
DC forward current	I_F			600	A
Peak forward current	I_{FRM}	t_p = 1ms		1200	A
Total power dissipation	P_{tot}	T_c = 25 °C, per diode		4760	W
Surge current	I_{FSM}	V_R = 0 V, T_{vj} = 125 °C, t_p = 10 ms, half-sinewave		6000	A
Isolation voltage	V_{isol}	1 min, f = 50 Hz		10200	V
Junction temperature	T_{vj}			125	°C
Junction operating temperature	$T_{vj(op)}$		-40	125	°C
Case temperature	T_c		-40	125	°C
Storage temperature	T_{stg}		-40	125	°C

[1] Maximum rated values indicate limits beyond which damage to the device may occur per IEC 60747

ABB Switzerland Ltd, Semiconductors reserves the right to change specifications without notice.

Diode characteristic values [2]

Parameter	Symbol	Conditions		min	typ	max	Unit
Forward voltage [3]	V_F	I_F = 600 A	T_{vj} = 25 °C		3.2	3.8	V
			T_{vj} = 125 °C		3.4	4.0	
Continuous reverse current	I_R	V_R = 6500 V	T_{vj} = 25 °C			6	mA
			T_{vj} = 125 °C		35	75	
Reverse recovery current	I_{rr}	V_R = 3600 V, I_F = 600 A, V_{GE} = ±15 V, di/dt = 2500 A/µs L_σ = 280 nH inductive load, switch:	T_{vj} = 25 °C		790		A
			T_{vj} = 125 °C		990		
Recovered charge	Q_{rr}		T_{vj} = 25 °C		700		µC
			T_{vj} = 125 °C		1200		
Reverse recovery time	t_{rr}		T_{vj} = 25 °C		1700		ns
			T_{vj} = 125 °C		2200		
Reverse recovery energy	E_{rec}		T_{vj} = 25 °C		1100		mJ
			T_{vj} = 125 °C		2200		
Module stray inductance	$L_{\sigma\,AC}$	per diode			36		nH
Resistance, terminal-chip	$R_{AA'+CC'}$	per diode	T_C = 25 °C		0.2		mΩ
			T_C = 125 °C		0.3		

[2] Characteristic values according to IEC 60747 – 2
[3] Forward voltage is given at chip level

Thermal properties [4]

Parameter	Symbol	Conditions	min	typ	max	Unit
Diode thermal resistance junction to case	$R_{th(j-c)DIODE}$				0.021	K/W
Diode thermal resistance [5] case to heatsink	$R_{th(c-s)DIODE}$	diode per switch, λ grease = 1W/m × K		0.018		K/W

Mechanical properties [4]

Parameter	Symbol	Conditions		min	typ	max	Unit
Dimensions	L × W × H	Typical , see outline drawing			130 × 140 × 48		mm
Clearance distance in air	d_a	according to IEC 60664-1 and EN 50124-1	Term. to base:	40			mm
			Term. to term:	26			
Surface creepage distance	d_s	according to IEC 60664-1 and EN 50124-1	Term. to base:	64			mm
			Term. to term:	56			
Comparative tracking index	CTI				≥ 600		
Mounting torques [5]	M_s	Base-heatsink, M6 screws		4		6	Nm
	M_{t1}	Main terminals, M8 screws		8		10	
Mass	m				1150		g

[4] Thermal and mechanical properties according to IEC 60747 – 15
[5] For detailed mounting instructions refer to ABB document no. 5SYA 2039 - 01
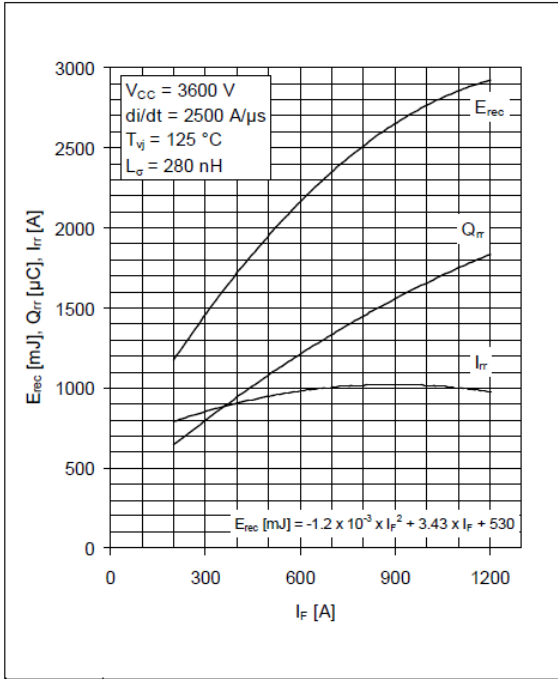
Electrical configuration
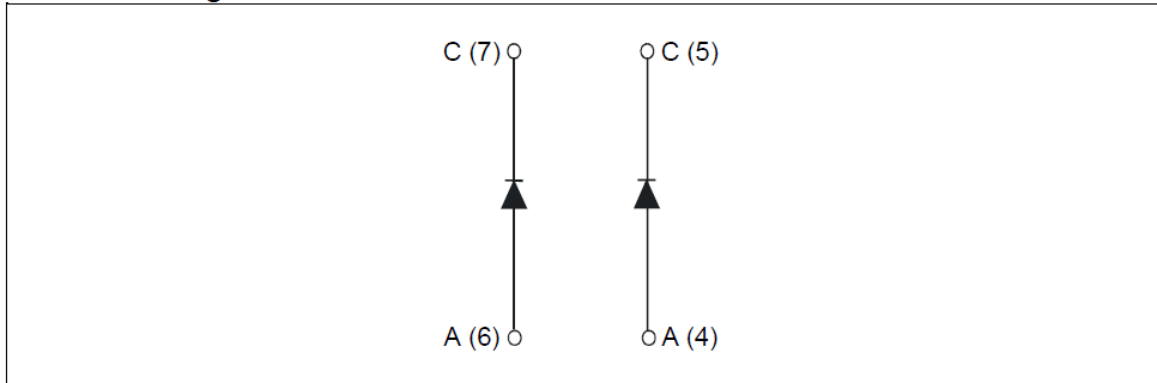
C (7) ○━━━━━━━━━━━○ C (5)

A (6) ○━━━━━━━━━━━○ A (4)

Outline drawing [5]
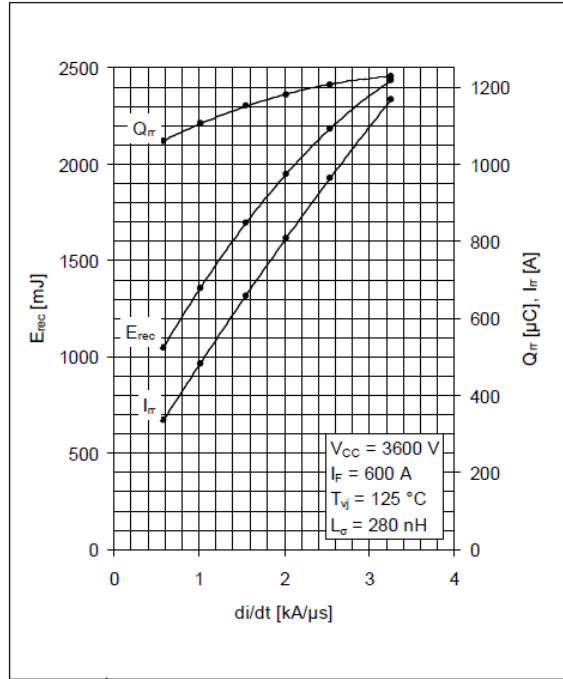
Note: all dimensions are shown in mm
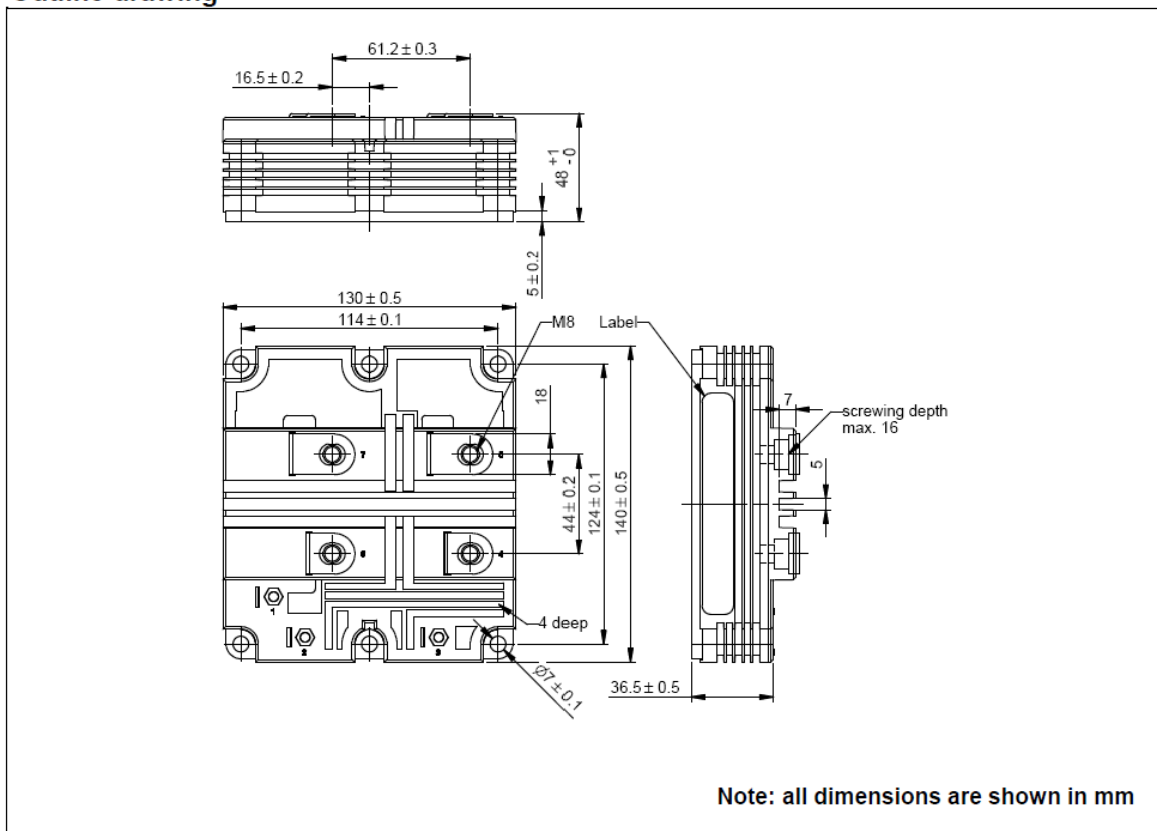
[5] For detailed mounting instructions refer to ABB document no. 5SYA 2039 - 01
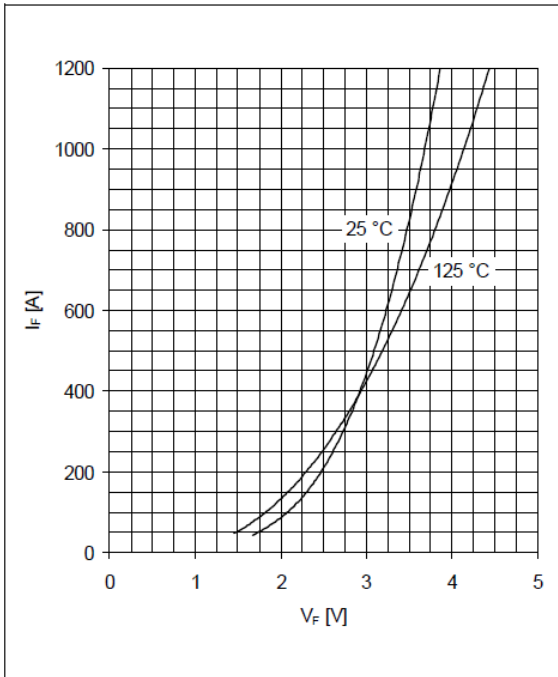
This is an electrostatic sensitive device, please observe the international standard IEC 60747-1, chap. IX. This product has been designed and qualified for industrial level.
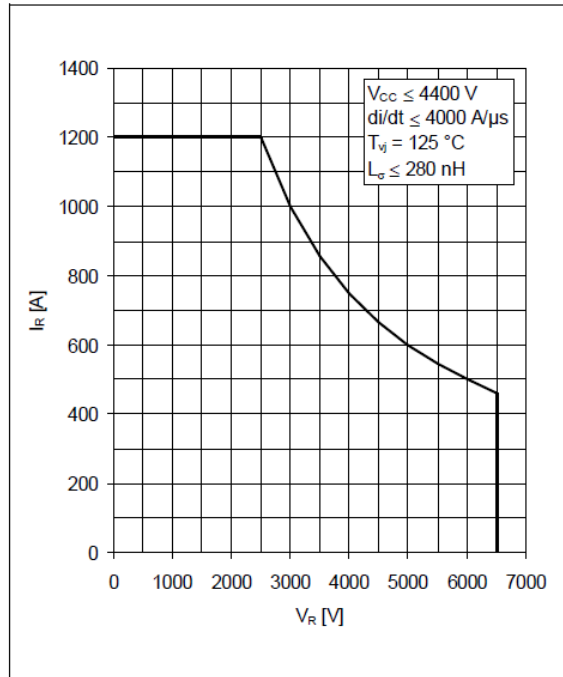
Fig. 1   Typical reverse recovery characteristics vs forward current

Fig. 2   Typical reverse recovery characteristics vs di/dt

Fig. 3   Typical diode forward characteristics, chip level

Fig. 4   Safe operating area diode (SOA)
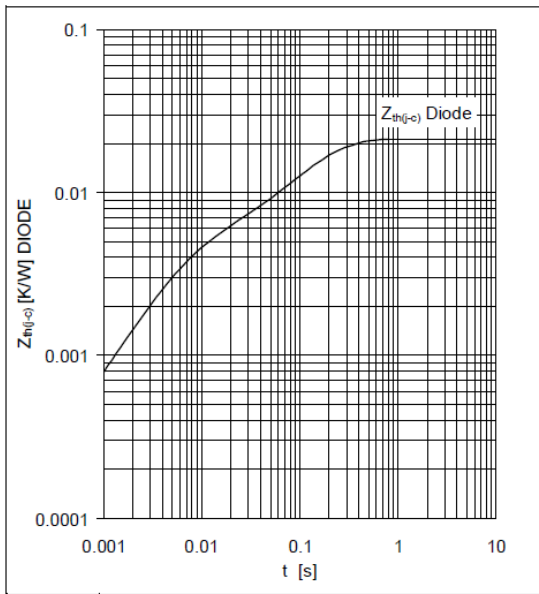
Fig. 5 Thermal impedance vs time

Analytical function for transient thermal impedance:

$$Z_{th\,(j\text{-}c)}(t) = \sum_{i=1}^{n} R_i\left(1 - e^{-t/\tau_i}\right)$$

	i	1	2	3	4	5
DIODE	R_i(K/kW)	17	4.2			
	τ_i(ms)	144	5.83			

For detailed information refer to:
- 5SYA 2042 Failure rates of HiPak modules due to cosmic rays
- 5SYA 2043 Load – cycle capability of HiPaks
- 5SYA 2045 Thermal runaway during blocking
- 5SYA 2058 Surge currents for IGBT diodes
- 5SZK 9120 Specification of environmental class for HiPak

| V_{CE} | = | 4500 V |
| I_C | = | 1200 A |

ABB HiPak™

IGBT Module
5SNA 1200G450300
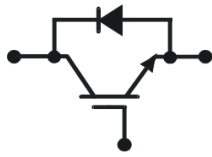
- **Ultra low-loss, rugged SPT$^+$ chip-set**
- **Smooth switching SPT$^+$ chip-set for good EMC**
- **Industry standard package**
- **High power density**
- **AlSiC base-plate for high power cycling capability**
- **AlN substrate for low thermal resistance**

Maximum rated values [1]

Parameter	Symbol	Conditions	min	max	Unit
Collector-emitter voltage	V_{CES}	V_{GE} = 0 V		4500	V
DC collector current	I_C	T_c = 85 °C		1200	A
Peak collector current	I_{CM}	t_p = 1 ms, T_c = 85 °C		2400	A
Gate-emitter voltage	V_{GES}		-20	20	V
Total power dissipation	P_{tot}	T_c = 25 °C, per switch (IGBT)		10500	W
DC forward current	I_F			1200	A
Peak forward current	I_{FRM}			2400	A
Surge current	I_{FSM}	V_R = 0 V, T_{vj} = 125 °C, t_p = 10 ms, half-sinewave		9000	A
IGBT short circuit SOA	t_{psc}	V_{CC} = 3400 V, $V_{CEM\,CHIP} \leq$ 4500 V $V_{GE} \leq$ 15 V, $T_{vj} \leq$ 125 °C		10	µs
Isolation voltage	V_{isol}	1 min, f = 50 Hz		7400	V
Junction temperature	T_{vj}			125	°C
Junction operating temperature	$T_{vj(op)}$		-40	125	°C
Case temperature	T_c		-40	125	°C
Storage temperature	T_{stg}		-40	125	°C
Mounting torques [2]	M_s	Base-heatsink, M6 screws	4	6	Nm
	M_{t1}	Main terminals, M8 screws	8	10	
	M_{t2}	Auxiliary terminals, M4 screws	2	3	

[1] Maximum rated values indicate limits beyond which damage to the device may occur per IEC 60747
[2] For detailed mounting instructions refer to ABB Document No. 5SYA2039

ABB Switzerland Ltd, Semiconductors reserves the right to change specifications without notice.

IGBT characteristic values [3]

Parameter	Symbol	Conditions		min	typ	max	Unit
Collector (-emitter) breakdown voltage	$V_{(BR)CES}$	$V_{GE} = 0$ V, $I_C = 10$ mA, $T_{vj} = 25$ °C		4500			V
Collector-emitter [4] saturation voltage	$V_{CE\,sat}$	$I_C = 1200$ A, $V_{GE} = 15$ V	$T_{vj} = 25$ °C		2.6		V
			$T_{vj} = 125$ °C		3.55		V
Collector cut-off current	I_{CES}	$V_{CE} = 4500$ V, $V_{GE} = 0$ V	$T_{vj} = 25$ °C			12	mA
			$T_{vj} = 125$ °C			120	mA
Gate leakage current	I_{GES}	$V_{CE} = 0$ V, $V_{GE} = \pm20$ V, $T_{vj} = 125$ °C		-500		500	nA
Gate-emitter threshold voltage	$V_{GE(TO)}$	$I_C = 240$ mA, $V_{CE} = V_{GE}$, $T_{vj} = 25$ °C		4.5		6.5	V
Gate charge	Q_{ge}	$I_C = 1200$ A, $V_{CE} = 2800$ V, $V_{GE} = -15$ V .. 15 V			8.86		µC
Input capacitance	C_{ies}	$V_{CE} = 25$ V, $V_{GE} = 0$ V, f = 1 MHz, $T_{vj} = 25$ °C			120		nF
Output capacitance	C_{oes}				6.02		
Reverse transfer capacitance	C_{res}				2.58		
Turn-on delay time	$t_{d(on)}$	$V_{CC} = 2800$ V, $I_C = 1200$ A, $R_G = 1.5$ Ω, $C_{GE} = 220$ nF, $V_{GE} = \pm15$ V, $L_\sigma = 150$ nH, inductive load	$T_{vj} = 25$ °C		740		ns
			$T_{vj} = 125$ °C		750		
Rise time	t_r		$T_{vj} = 25$ °C		210		ns
			$T_{vj} = 125$ °C		230		
Turn-off delay time	$t_{d(off)}$	$V_{CC} = 2800$ V, $I_C = 1200$ A, $R_G = 1.5$ Ω, $C_{GE} = 220$ nF, $V_{GE} = \pm15$ V, $L_\sigma = 150$ nH, inductive load	$T_{vj} = 25$ °C		2280		ns
			$T_{vj} = 125$ °C		2470		
Fall time	t_f		$T_{vj} = 25$ °C		600		ns
			$T_{vj} = 125$ °C		660		
Turn-on switching energy	E_{on}	$V_{CC} = 2800$ V, $I_C = 1200$ A, $R_G = 1.5$ Ω, $C_{GE} = 220$ nF, $V_{GE} = \pm15$ V, $L_\sigma = 150$ nH, inductive load	$T_{vj} = 25$ °C		3080		mJ
			$T_{vj} = 125$ °C		4350		
Turn-off switching energy	E_{off}	$V_{CC} = 2800$ V, $I_C = 1200$ A, $R_G = 1.5$ Ω, $C_{GE} = 220$ nF, $V_{GE} = \pm15$ V, $L_\sigma = 150$ nH, inductive load	$T_{vj} = 25$ °C		4960		mJ
			$T_{vj} = 125$ °C		6000		
Short circuit current	I_{SC}	$t_{psc} \leq 10$ µs, $V_{GE} = 15$ V, $T_{vj} = 125$ °C, $V_{CC} = 3400$ V, $V_{CEM\,CHIP} \leq 4500$ V			5200		A
Module stray inductance	$L_{\sigma\,CE}$				18		nH
Resistance, terminal-chip	$R_{CC'+EE'}$		$T_C = 25$ °C		0.07		mΩ
			$T_C = 125$ °C		0.1		

[3] Characteristic values according to IEC 60747 – 9
[4] Collector-emitter saturation voltage is given at chip level

Diode characteristic values [5]

Parameter	Symbol	Conditions		min	typ	max	Unit
Forward voltage [6]	V_F	$I_F = 1200$ A	$T_{vj} = 25\ °C$		3.2		V
			$T_{vj} = 125\ °C$		3.5		
Reverse recovery current	I_{rr}		$T_{vj} = 25\ °C$		1460		A
		$V_{CC} = 2800$ V,	$T_{vj} = 125\ °C$		1600		
Recovered charge	Q_{rr}	$I_F = 1200$ A,	$T_{vj} = 25\ °C$		1030		µC
		$V_{GE} = \pm15$ V,	$T_{vj} = 125\ °C$		1660		
		$R_G = 1.5\ \Omega,$	$T_{vj} = 25\ °C$		1270		ns
Reverse recovery time	t_{rr}	$C_{GE} = 220$ nF,	$T_{vj} = 125\ °C$		1860		
		$L_\sigma = 150$ nH	$T_{vj} = 25\ °C$		1630		mJ
Reverse recovery energy	E_{rec}	inductive load	$T_{vj} = 125\ °C$		2730		

[5] Characteristic values according to IEC 60747 – 2
[6] Forward voltage is given at chip level

Package properties [7]

Parameter	Symbol	Conditions	min	typ	max	Unit
IGBT thermal resistance junction to case	$R_{th(j-c)IGBT}$				0.0095	K/W
Diode thermal resistance junction to case	$R_{th(j-c)DIODE}$				0.019	K/W
IGBT thermal resistance [2] case to heatsink	$R_{th(c-s)IGBT}$	IGBT per switch, λ grease = 1W/m × K		0.009		K/W
Diode thermal resistance [7] case to heatsink	$R_{th(c-s)DIODE}$	Diode per switch, λ grease = 1W/m × K		0.018		K/W
Partial discharge extinction voltage	V_e	f = 50 Hz, $Q_{PD} \leq 10pC$ (acc. to IEC 61287)	3500			V
Comparative tracking index	CTI			≥ 600		

[2] For detailed mounting instructions refer to ABB Document No. 5SYA2039

Mechanical properties [7]

Parameter	Symbol	Conditions		min	typ	max	Unit
Dimensions	L × W × H	Typical , see outline drawing			190 × 140 × 48		mm
Clearance distance in air	d_a	according to IEC 60664-1 and EN 50124-1	Term. to base:	40			mm
			Term. to term:	26			
Surface creepage distance	d_s	according to IEC 60664-1 and EN 50124-1	Term. to base:	64			mm
			Term. to term:	56			
Mass	m				1760		g

[7] Package and mechanical properties according to IEC 60747 – 15

Electrical configuration

Outline drawing [2]

Note: all dimensions are shown in mm
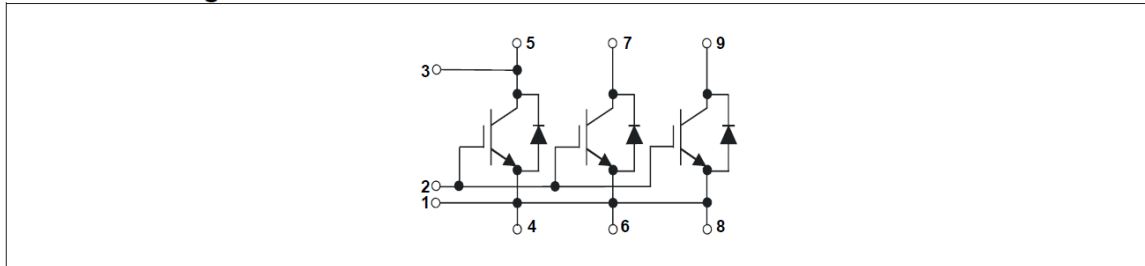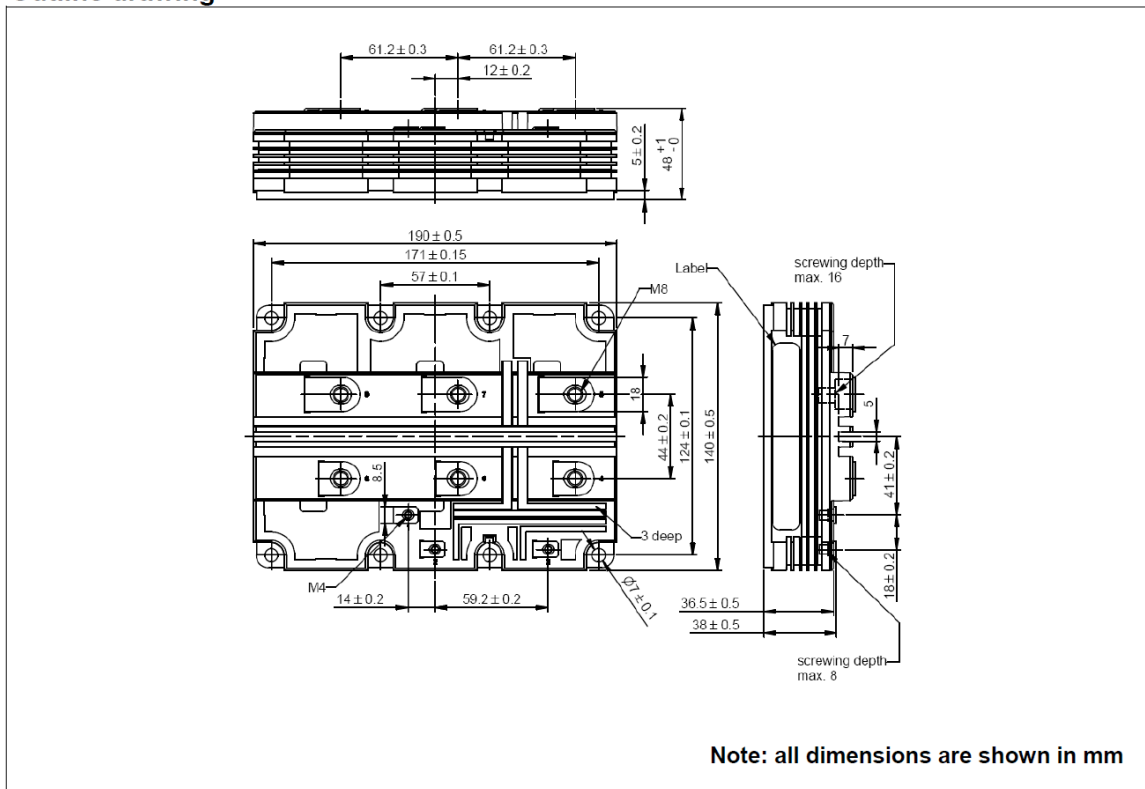
[2] For detailed mounting instructions refer to ABB Document No. 5SYA2039

This is an electrostatic sensitive device, please observe the international standard IEC 60747-1, chap. IX.

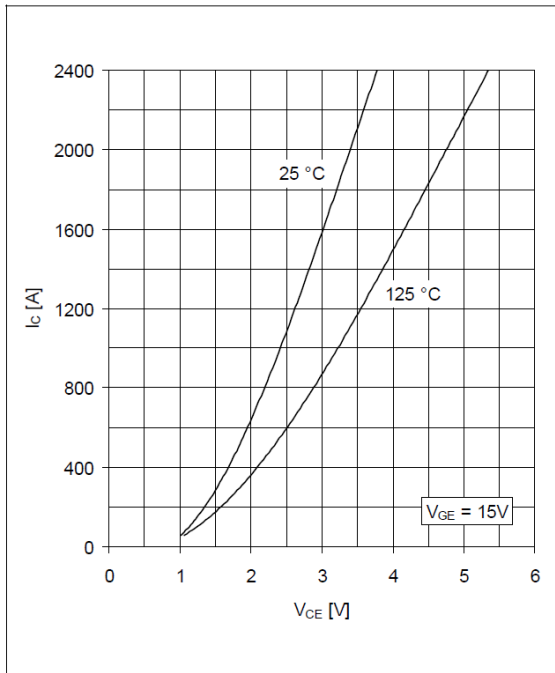**This product has been designed and qualified for Industrial Level.**

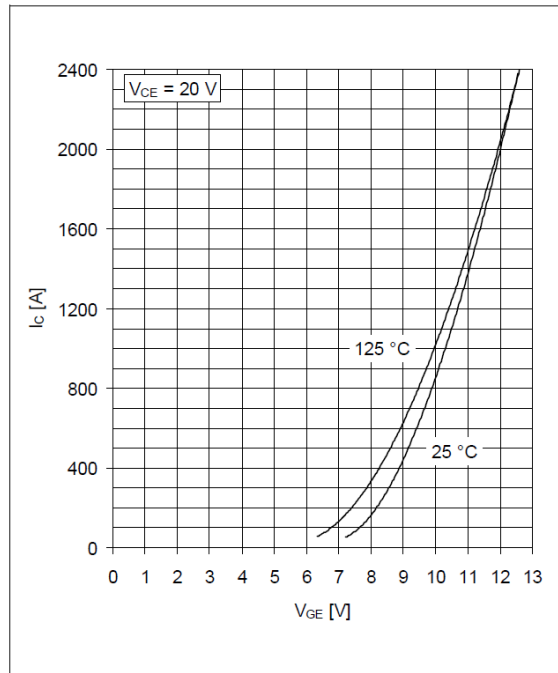**Fig. 1**   Typical on-state characteristics, chip level
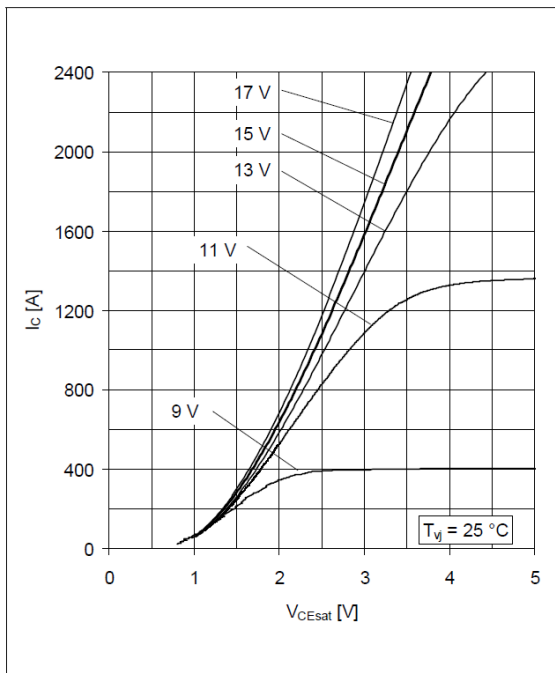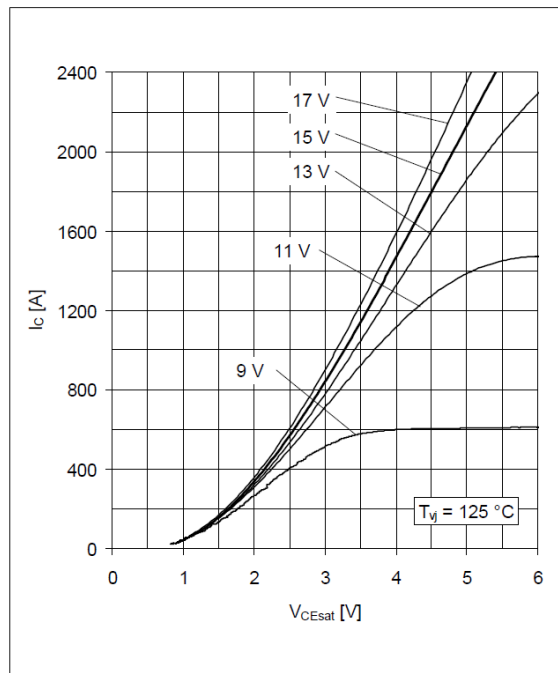
Fig. 2   Typical transfer characteristics, chip level

Fig. 3   Typical output characteristics, chip level

Fig. 4   Typical output characteristics, chip level
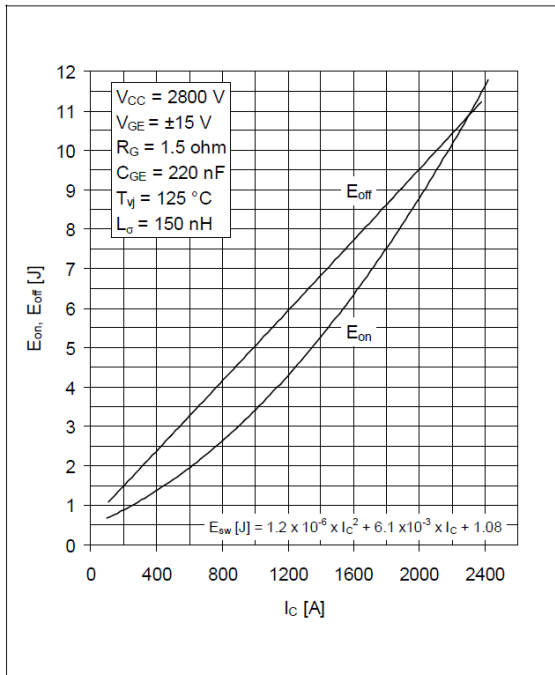
Fig. 5   Typical switching energies per pulse
         vs collector current
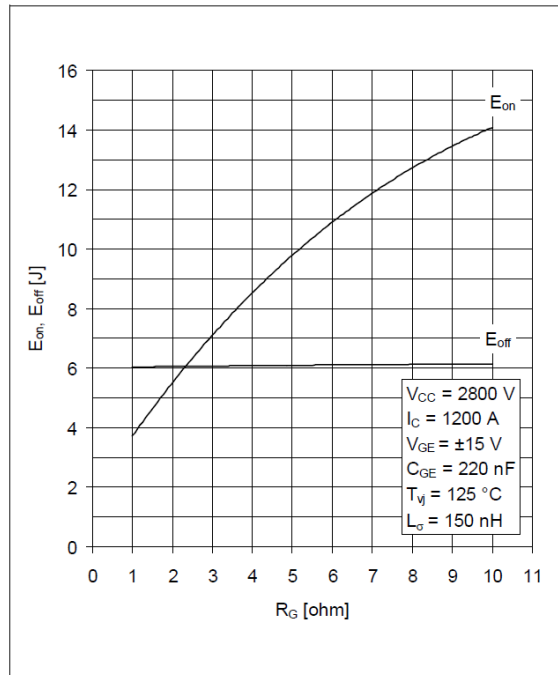
Fig. 6   Typical switching energies per pulse
         vs gate resistor
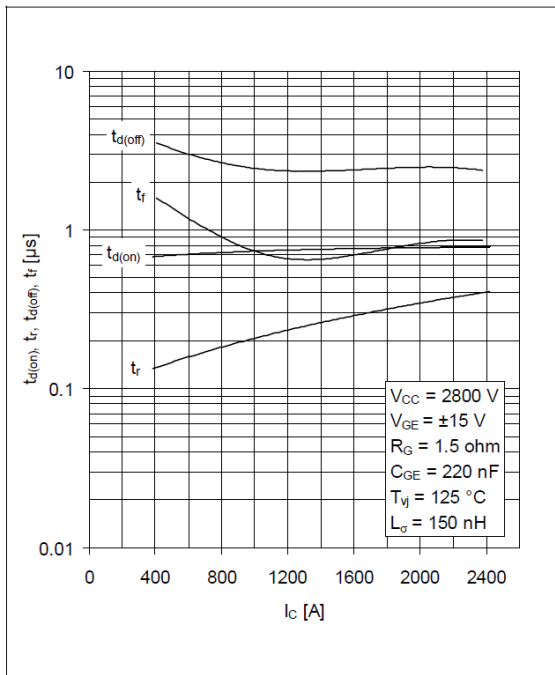
Fig. 7   Typical switching times
         vs collector current
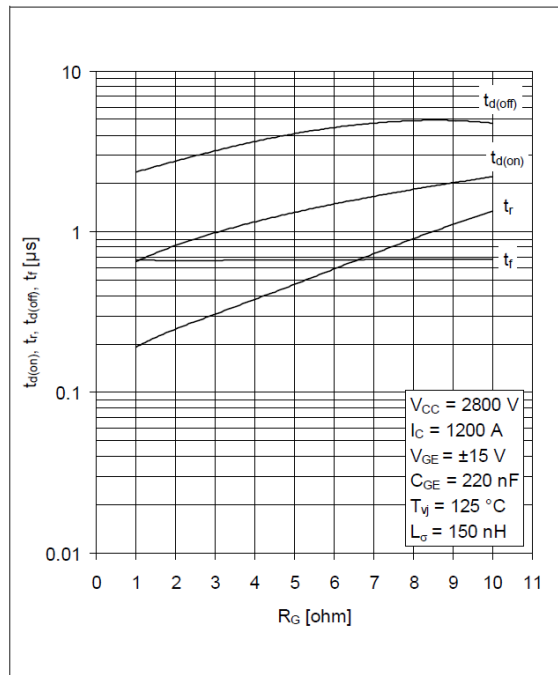
Fig. 8   Typical switching times
         vs gate resistor
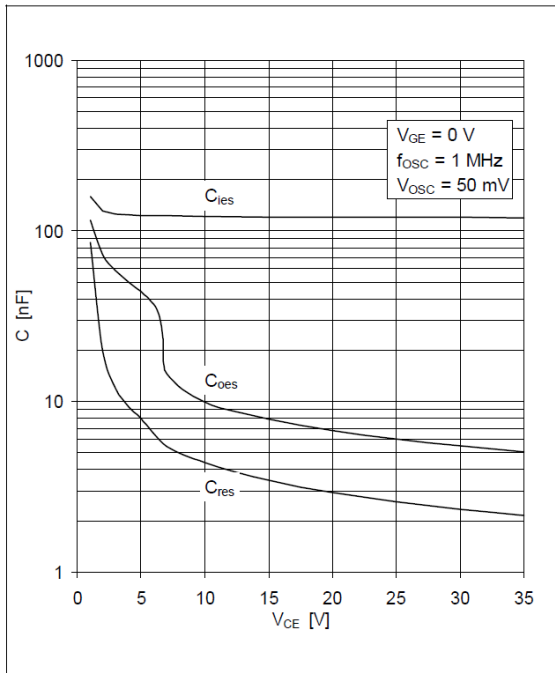
Fig. 9 Typical capacitances
vs collector-emitter voltage
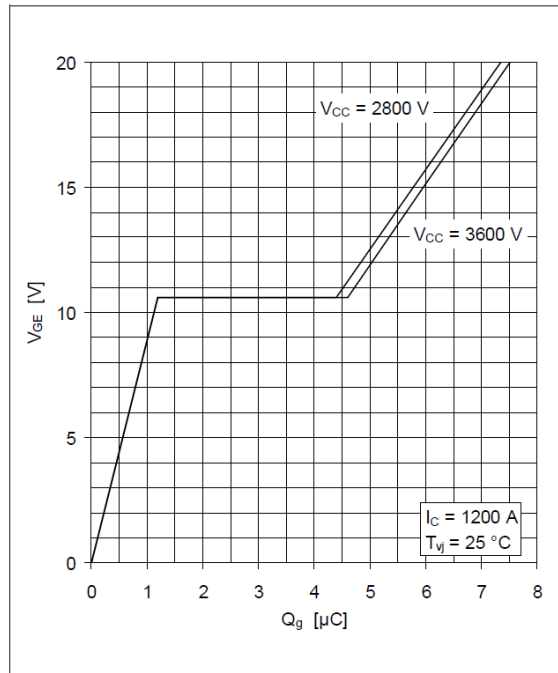
Fig. 10 Typical gate charge characteristics
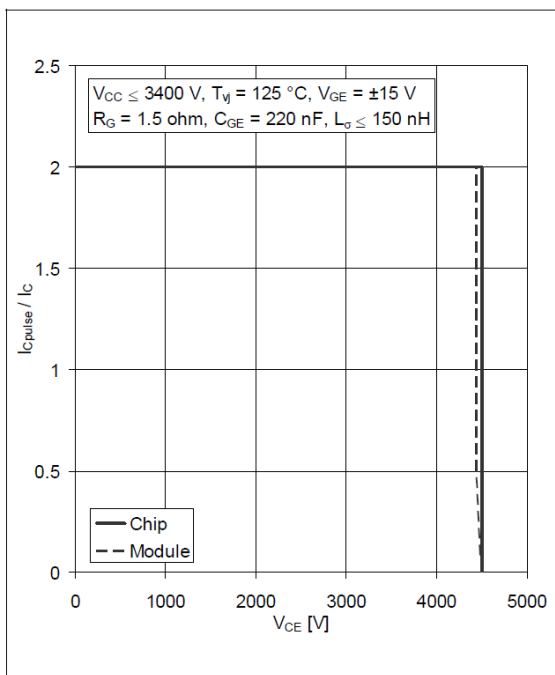
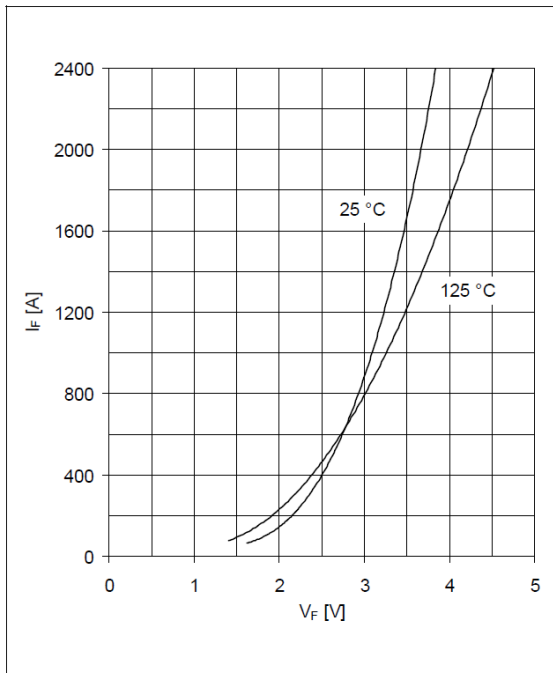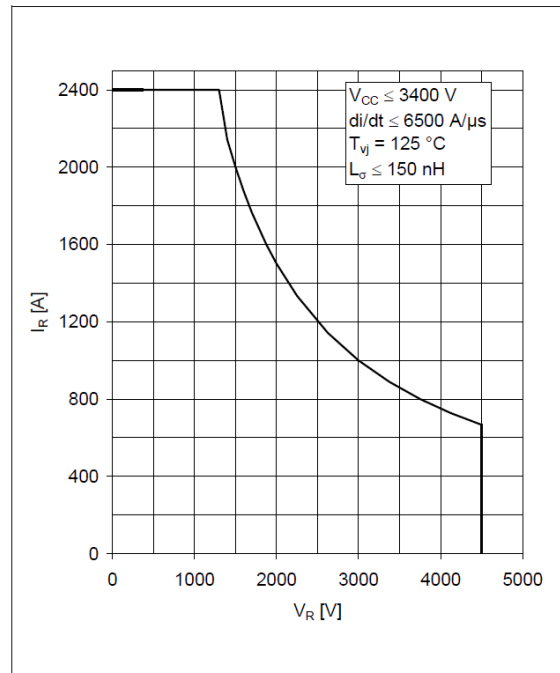**Fig. 11** Turn-off safe operating area (RBSOA)

ABB Switzerland Ltd, Semiconductors reserves the right to change specifications without notice.

Fig. 12 Typical reverse recovery characteristics vs forward current

$$E_{rec} [mJ] = -5.25 \times 10^{-4} \times I_F{}^2 + 2.61 \times I_F + 375$$
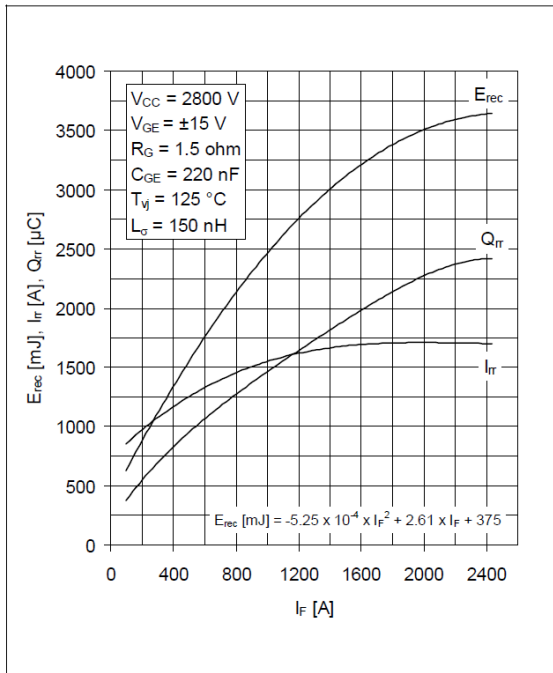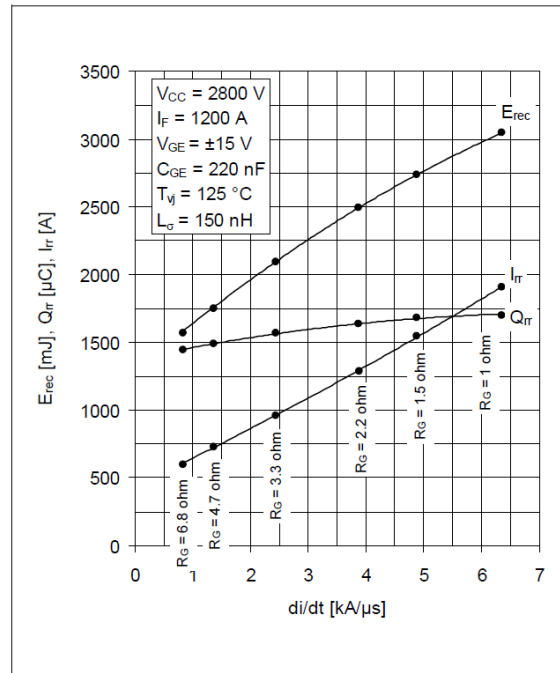
Fig. 13 Typical reverse recovery characteristics vs di/dt

Fig. 14 Typical diode forward characteristics, chip level

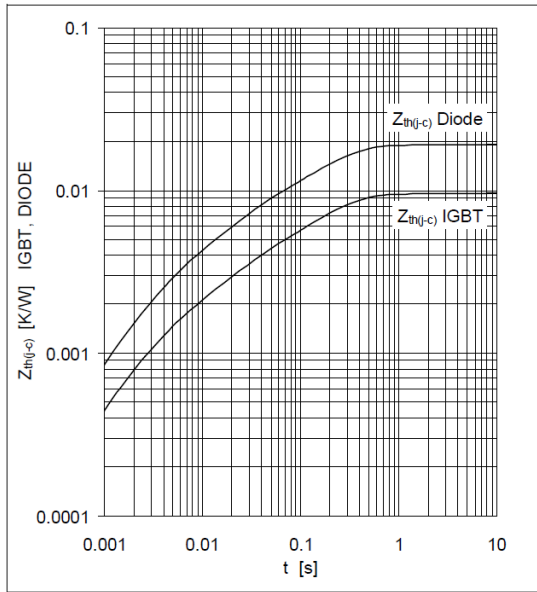**Fig. 15** Safe operating area diode (SOA)

Fig. 16 Thermal impedance vs time

Analytical function for transient thermal impedance:

$$Z_{th\,(j\text{-}c)}(t) = \sum_{i=1}^{n} R_i\left(1 - e^{-t/\tau_i}\right)$$

	i	1	2	3	4	5
IGBT	R_i(K/kW)	6.36	2.11	1.04		
	τ_i(ms)	193	21.4	2.78		
DIODE	R_i(K/kW)	12.5	4.37	2.16		
	τ_i(ms)	192	22.6	3.1		

For detailed information refer to:
- 5SYA 2042 Failure rates of HiPak modules due to cosmic rays
- 5SYA 2043 Load – cycle capability of HiPaks
- 5SYA 2045 Thermal runaway during blocking
- 5SYA 2053 Applying IGBT
- 5SZK 9120 Specification of environmental class for HiPak